Supporting Information for Mechanistic Dissection Reveals Striking Specificity within Dynamic Transcriptional Protein-Protein Complexes

Protein Expression and Purification

Med25 AcID was expressed and purified from a pET21b-Med25(394-543)-His_6 plasmid from E. coli BL21 (DE3) cells as described previously.(1) Briefly, 50 mL starter cultures in LB were grown overnight in the presence of 0.1 mg/mL ampicillin (Gold Bio Technology) at 37 ºC at 150 rpm. The next day, 5 mL of the starter culture was used to inoculate 1 L of TB media (24 g yeast extract, 12 g tryptone, 4 mL glycerol, 100 mL 0.17 M KH_2PO_4/0.72 M K_2HPO_4, 900 mL water) with 0.1 mg/mL ampicillin, which was grown at 37 ºC, 250 rpm, to an OD_{600} of 0.8. The incubator temperature was lowered to 21 ºC and the culture was allowed to recover for 30 min, at which point isopropyl β-D1-thiogalactopyranoside (IPTG, Research Products International) was added to a final concentration of 500 μM to induce expression. The protein was allowed to express overnight (~18 hr), after which the cells were harvested via centrifugation (6000 rpm, 20 min), and then frozen and stored at –80 ºC. Uniformly ^{13}C,^{15}N labeled Med25 for NMR experiments was expressed identically except using M9 minimal media supplemented with 1 g/L $^{15}NH_4Cl$, 2 g/L ^{13}C-$_D$-glucose, and 0.5% ^{13}C,^{15}N-labelled Bioexpress media for the 1 L growth (all labeled components were purchased from Cambridge Isotopes).

To purify Med25, cell pellets were resuspended in 25 mL lysis buffer (50 mM phosphate, 300 mM NaCl, 10 mM imidazole, pH 7.2, 1.4 μL/mL β-mercaptoethanol, 1 Roche complete mini protease inhibitor tablet) and lysed by sonication. Insoluble material was then pelleted by centrifugation (9500 rpm, 20 min), the supernatant was removed and re-sonicated, and then filtered using a 0.45 syringe filter (CellTreat) and loaded onto an AKTA Pure FPLC equipped with a Ni HisTrap HP column (GE Healthcare) pre-equilibrated with wash buffer (50 mM phosphate, 300 mM NaCl, 10 mM imidazole, pH 7.2). Med25 was then purified using a gradient of 10–300 mM imidazole (other buffer components were constant), and fractions containing Med25 were pooled and subjected to secondary purification using a HiTrap SP HP cation exchange column (GE Healthcare) using a gradient of 0–1 M NaCl (50 mM sodium phosphate, 1 mM DTT, pH 6.8). Pooled fractions were dialyzed into stopped-flow buffer (10 mM sodium phosphate, 100 mM NaCl, 1% glycerol, 0.001% NP-40, pH 6.8) or NMR buffer (20 mM sodium phosphate, 150 mM NaCl, pH 6.5). Concentration was determined by a NanoDrop instrument using an extinction coefficient at 280 nm of 22,460 $M^{-1}cm^{-1}$. Aliquots were flash frozen in liquid

N_2 and stored at –80 ºC until use. Protein identity was confirmed by mass spectrometry (Agilent Q-TOF).

Peptide Synthesis

The peptides used in this study were prepared using standard Fmoc solid-phase peptide synthesis on a Liberty Blue Microwave Peptide Synthesizer (CEM). Deprotection was accomplished by 20% piperidine (ChemImpex) in DMF supplemented with 0.2 M Oxyma Pure (CEM), with irradiation at 90 ºC for 1 min. Coupling reactions were completed with 5 equivalents of Fmoc-amino acid (CEM), 7 equivalents of diisopropylcarbodiimide (ChemImpex), and 5 equivalents of Oxyma Pure in DMF, with irradiation at 90 ºC for 4 min. Between steps, the resin was rinsed four times with an excess of DMF. Selectively ^{15}N-labeled peptides were synthesized using Fmoc-^{15}N-Leu in place of Fmoc-Leu in the specified positions.

Unlabeled peptides were acetylated at the *N*-terminus through reaction of a mixture of acetic anhydride (Sigma), triethylamine (Sigma), and dichloromethane in a 1:1:8 ratio for 30 min after the conclusion of the synthesis. 4-DMN labeled peptides were coupled with ~1.5 equivalents of 4-DMN-β-Alanine, as described previously.(1) All peptides were cleaved from the resin using a cocktail of 95:2.5:2.5 trifluoroacetic acid (Sigma), ethanedithiol (Sigma), and water for 3 hr, followed by filtration. The peptide solution was concentrated under a stream of N_2, then precipitated with cold diethyl ether and pelleted by centrifugation (4,500 rpm, 5 min). The ether was then discarded and the pellet was taken up in 7:3 100 mM Ammonium acetate-acetonitrile. The peptide was purified by an Agilent 1260 preparatory HPLC using a 40 minute gradient of 10-50% acetonitrile, with 100 mM ammonium acetate as the stationary phase. The flow rate was 40 mL/min. Fractions containing the correct peptide were pooled and lyophilized, and the resulting powders were dissolved in minimal DMSO and stored at –20 ºC. Concentrations were taken with a 1:100 dilution of the DMSO stock into 6 M Guanidinium Chloride on a NanoDrop instrument, using extinction coefficients of 5,690 $M^{-1}cm^{-1}$ (280 nm, unlabeled) or 10,800 $M^{-1}cm^{-1}$ (450 nm, 4-DMN-labeled). Identity of the peptides were confirmed by mass spectrometry.

Table S1. Sequences of peptides used for this study

Peptide	Sequence
ETV1	Ac-DLAHDSEELFQDLSQLQETWLAEAQVPDNDEQ
ETV4	Ac-LPPLDSEDLFQDLSHFQETWLAEAQVPDSDEQ
ETV5	Ac-DLAHDSEELFQDLSQLQEAWLAEAQVPDDEQ
4-DMN-ETV1	4-DMN-βAla-DLAHDSEELFQDLSQLQETWLAEAQVPDNDEQ
4-DMN-ETV4	4-DMN-βAla-LPPLDSEDLFQDLSHFQETWLAEAQVPDSDEQ
4-DMN-ETV5	4-DMN-βAla-DLAHDSEELFQDLSQLQEAWLAEAQVPDDEQ
4-DMN-ETV4$^{LPPL/HL}$	4-DMN-βAla-LPPLDSEDLFQDLSHLQETWLAEAQVPDSDEQ
4-DMN-ETV4$^{LPPL/QL}$	4-DMN-βAla-LPPLDSEDLFQDLSQLQETWLAEAQVPDSDEQ
4-DMN-ETV4$^{DLAH/HL}$	4-DMN-βAla-DLAHDSEDLFQDLSHLQETWLAEAQVPDSDEQ
4-DMN-ETV4$^{DLAH/HF}$	4-DMN-βAla-DLAHDSEDLFQDLSHFQETWLAEAQVPDSDEQ
4-DMN-ETV4$^{DLAH/QF}$	4-DMN-βAla-DLAHDSEDLFQDLSQFQETWLAEAQVPDSDEQ
4-DMN-ETV1$^{\Delta Nt}$	4-DMN-βAla-DSEELFQDLSQLQETWLAEAQVPDNDEQ
4-DMN-ETV4$^{\Delta Nt}$	4-DMN-βAla-DSEDLFQDLSHFQETWLAEAQVPDSDEQ
ETV1^{Q52H}	Ac-DLAHDSEELFQDLSHLQETWLAEAQVPDNDEQ
ETV4^{H59Q}	Ac-LPPLDSEDLFQDLSQFQETWLAEAQVPDSDEQ
ETV1^{L39V}	Ac-DVAHDSEELFQDLSQLQETWLAEAQVPDNDEQ
ETV4^{L48V}	Ac-LPPVDSEDLFQDLSHFQETWLAEAQVPDSDEQ
ETV4^{F60L}	Ac-LPPLDSEDLFQDLSHLQETWLAEAQVPDSDEQ

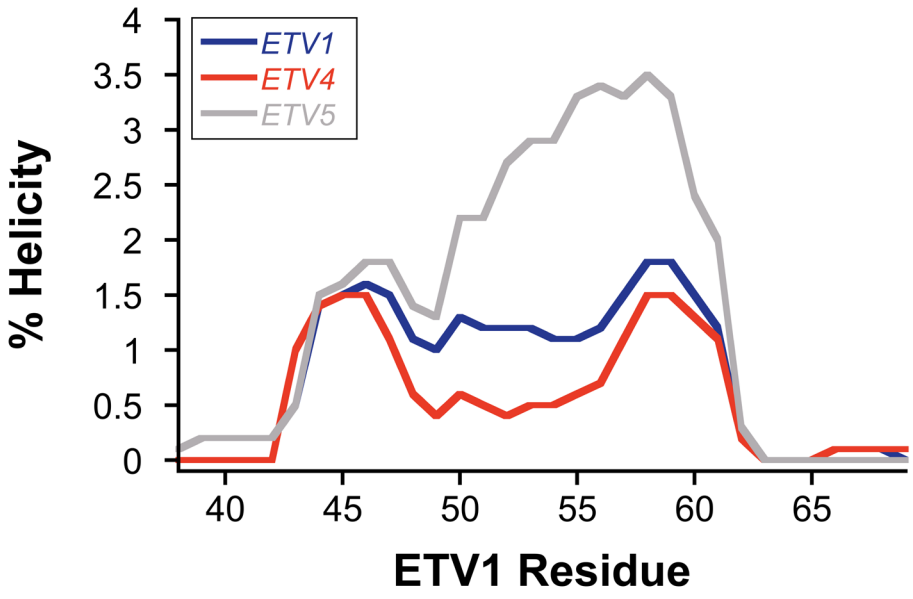

Figure S1. Predicted helical propensity of PEA3 activators from Agadir,(2) aligned to ETV1 sequence.

Stopped-flow kinetics

Stopped-flow kinetic assays were performed using a Kintek SF-2001 stopped flow instrument equipped with a 100-W Xe arc lamp in two-syringe mode. All experiments were completed at 10 ºC in stopped-flow buffer (10 mM sodium phosphate, 100 mM NaCl, 2% DMSO, 1% glycerol, 0.001% NP-40, pH 6.8). All concentrations reported are after mixing. The 4-DMN fluorophore was excited at 440 nm, and fluorescence intensity was measured at wavelengths >510 nm using a long-pass filter (Corion). Association experiments were completed by 1:1 mixing of a constant concentration of 0.25 μM 4-DMN-labeled peptide with variable concentrations of Med25. Dissociation experiments were performed by mixing 50 μM unlabeled peptide with a preformed complex of 0.5-1 μM Med25 and 0.25 μM labeled peptide. Unlabeled peptides for dissociation experiments mutants were typically the parent peptide, but no unique effects were observed from using different competitors. Typically, 30-40 traces were averaged before fitting.

Traces were fitted using a series of exponential equations (first equation below), where $F(t)$ is the fluorescence at time t, F_∞ is the endpoint fluorescence, ΔF_n are the fluorescence amplitudes, and $k_{obs,n}$ are the observed rate constants. Equilibrium dissociation constants (K_d) were determined by fitting the concentration dependence of F_∞ values to a standard hyperbolic equation. The individual $k_{obs,n}$ values were plotted as a function of concentration and fit to square hyperbola (second equation below) to determine the maximal observed rate constant ($k_{obs,n,max}$), and the half maximal concentration ($K_{1/2,n}$). The value of $k_{obs,n,min}$ was included for fitting purposes, but the value itself is defined by the corresponding $k_{obs,n,off}$ value from dissociation experiments and thus the $k_{obs,n,min}$ value from fitting was not used for calculations. The microscopic rate constants were calculated using a combined rapid equilibrium and steady-state approximation, detailed in the next section. This approach was enabled by optimized conditions for dissociation experiments from our previous report,(1) as the $k_{obs,n,off}$ phases were more clearly defined under the conditions used. Values of all microscopic rate and equilibrium constants were calculated for single datasets and averaged across 2-3 results from independent datasets. All errors reported are the standard deviation between the results from separate datasets. Examples of datasets for all mutants are reported at the end of this document.

$$F(t) = F_{\infty} + \sum \Delta F_n \exp\left(-k_{obs,n} \times t\right)$$

$$k_{obs,n} = \frac{k_{obs,n,max} * [Med25]}{[Med25] + K_{1/2,n}} + k_{obs,n,min}$$

Calculation of Microscopic Rate Constants

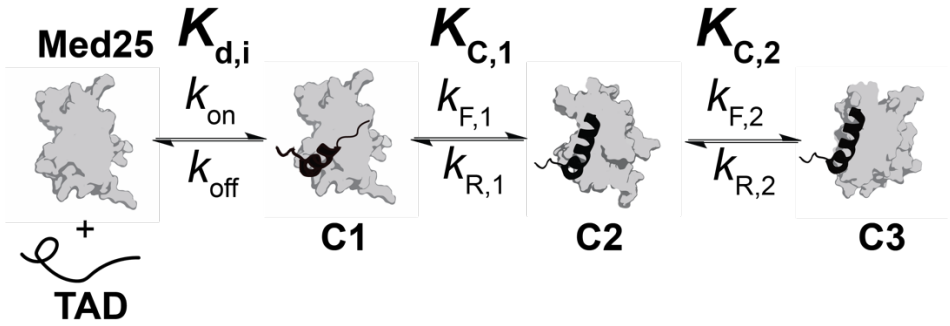

Figure S2. Kinetic mechanism of Med25 binding to PEA3 TADs, as determined previously.(1) Microscopic rate and equilibrium constants are labeled as they appear in this supporting information document.

Here, we chose to use a combined rapid equilibrium and steady state approach to determine rate parameters as a straightforward way to handle the large amount of complex kinetic data collected. This method for calculating the microscopic rate constants is split into two “sections”. First, the mechanism is considered as only the first two steps: the initial binding step to form conformer C1 and its transition to C2. After calculation of all first order microscopic rate constants from this “section” of the mechanism, the transition from C2 to C3 is considered. This is similar to treating the first two steps of the binding mechanism as a rapid equilibrium before the final conformational transition to C3. For all mechanisms where only a single conformational change was observed, the calculations followed the same procedure except that the final step to calculate rate constants for the C2–C3 transition was left out.

Beginning from the first two steps, the maximal observed rate constant of the first conformational change phase ($k_{obs,2,max}$) is:

$$k_{obs,2,max} = k_{F,1} + k_{R,1}$$

And, by the steady-state approximation, the corresponding observed rate constant for dissociation ($k_{obs,2,off}$) is:

$$k_{obs,2,off} = k_{R,1} \times \frac{k_{off}}{k_{off} + k_{F,1}}$$

The value of k_{off} can be retrieved from the observed rate constants from dissociation experiments ($k_{obs,n,off}$) in an analogous way to our previous work (1). That is, by the exact expression for a two step induced fit mechanism, k_{off} is equivalent to:

$$k_{off} = k_{obs,1,off} + k_{obs,2,off} - k_{obs,2,max}$$

In all cases except for ETV4, the fast dissociation phase ($k_{obs,1,off}$) is well defined in dissociation experiments, enabling the use of this method. For ETV4, where it is not well defined, this value was set to the minimal value we observed for other variants tested, 300 s^{-1}. To substitute a directly measurable value for $k_{F,1}$, the equation defined above for $k_{obs,2,max}$ can be used. Thus, by substitution and simplification:

$$k_{obs,2,off} = k_{R,1} \times \frac{k_{obs,1,off} + k_{obs,2,off} - k_{obs,2,max}}{k_{obs,1,off} + k_{obs,2off} - k_{R,1}}$$

And by rearrangement:

$$k_{R,1} = \frac{k_{obs,2,off} \times (k_{obs,1,off} + k_{obs,2,off})}{k_{obs,1,off} + 2 \times k_{obs,2,off} - k_{obs,2,max}}$$

Calculation of $k_{F,1}$ is then obtained by subtracting the $k_{R,1}$ value from $k_{obs,2,max}$. Next, the transition from C2 to C3 was considered. In dissociation experiments, the observed rate constant of the kinetic phase corresponding to this step ($k_{obs,3,off}$) is given below by the steady-state approximation:

$$k_{obs,3,off} = k_{R,2} \times \frac{k_{R,1}{}'}{k_{R,1}{}' + k_{F,2}}$$

Here, $k_{R,1}$' is the net rate constant for successful dissociation from the C2 conformer and is identical to the expression for $k_{obs,2,off}$ above. Thus, the value of $k_{obs,2,off}$ that is obtained from fitting is used in this calculation. Similarly, $k_{obs,3,max}$ is the sum of $k_{F,2}$ and $k_{R,2}$. Thus, substitution in a analogous manner as above gives:

$$k_{obs,3,off} = k_{R,2} \times \frac{k_{obs,2,off}}{k_{obs,2,off} + k_{obs,3,max} - k_{R,2}}$$

And by rearrangement:

$$k_{R,2} = \frac{k_{obs,3,off} \times (k_{obs,2,off} + k_{obs,3,max})}{k_{obs,2,off} + k_{obs,3,off}}$$

Again, $k_{F,2}$ is obtained by subtracting the calculated value of $k_{R,2}$ from $k_{obs,3,max}$. The calculated values for all tested variants in this study are shown in Table S2. Relative populations of C1, C2, and C3 at equilibrium were then determined by the conformational equilibrium constants ($K_{C,n} = k_{F,n}/k_{R,n}$), which by definition are ratios between the conformational states. Below are the equations used to calculate the population of each conformational state, using C1 as the reference state. Only the relative conformational populations of the bound state were considered, thus the values are concentration-independent.

$$Population\ C1 = \frac{1}{1 + K_{C,1} + K_{C,1} \times K_{C,2}} \times 100\%$$

$$Population\ C2 = \frac{K_{C,1}}{1 + K_{C,1} + K_{C,1} \times K_{C,2}} \times 100\%$$

$$Population\ C3 = \frac{K_{C,1} \times K_{C,2}}{1 + K_{C,1} + K_{C,1} \times K_{C,2}} \times 100\%$$

Table S2 Calculated rate and equilibrium constants for all 4-DMN-labeled PEA3 TADs

ETV Variant	$K_{C,1}$	$k_{F,1}$ (s^{-1})	$k_{R,1}$ (s^{-1})	$K_{C,2}$	$k_{F,2}$ (s^{-1})	$k_{R,2}$ (s^{-1})	K_d (μM)
ETV1	3.6 ± 0.7	52 ± 5	15 ± 3	0.5 ± 0.1	2.4 ± 0.3	4.9 ± 0.8	1.2 ± 0.2
ETV4	3.2 ± 0.5	56 ± 8	18 ± 1	2.3 ± 0.5	3.3 ± 0.7	1.4 ± 0.1	0.7 ± 0.2
ETV5	3.4 ± 0.6	46 ± 4	14 ± 2	0.6 ± 0.3	2.5 ± 1.0	4.1 ± 0.3	0.9 ± 0.1
ETV4$^{DLAH/HL}$	2.7 ± 0.4	101 ± 7	38 ± 3	0.6 ± 0.1	4.6 ± 0.5	7.8 ± 0.1	1.2 ± 0.2
ETV4$^{DLAH/QF}$	5.4 ± 0.5	54 ± 6	10 ± 0.3	–	–	–	0.9 ± 0.1
ETV4$^{DLAH/HF}$	4.2 ± 0.2	63 ± 8	15 ± 2	–	–	–	0.8 ± 0.3
ETV4$^{LPPL/QL}$	0.7 ± 0.1	27 ± 4	37 ± 1	–	–	–	2.0 ± 0.1
ETV4$^{LPPL/HL}$	0.9 ± 0.1	34 + 2	38 ± 1	–	–	–	1.7 ± 0.1
ETV4$^{LPPL/QF}$	2.8 ± 0.4	52 ± 1	13 ± 1	1.6 ± 0.2	13 ± 0.7	8.1 ± 0.8	0.6 ± 0.1
ETV1$^{\Delta Nt}$	1.0 ± 0.3	21 ± 3	21 ± 3	–	–	–	0.7 ± 0.1
ETV4$^{\Delta Nt}$	3.9 ± 0.7	62 ± 1	16 ± 3	4.9 ± 1.5	4.9 ± 0.9	1.0 ± 0.1	0.4 ± 0.1

Table S3 Calculated conformational populations for all 4-DMN-labeled PEA3 TADs

ETV Variant	C1 Population (%)	C2 Population (%)	C3 Population (%)
ETV1	16 ± 2	56 ± 6	28 ± 5
ETV4	9 ± 1	28 ± 4	63 ± 5
ETV5	16 ± 2	53 ± 8	31 ± 9
ETV4$^{DLAH/HL}$	19 ± 2	51 ± 3	30 ± 2
ETV4$^{DLAH/QF}$	16 ± 1	84 ± 1	–
ETV4$^{DLAH/HF}$	19 ± 1	81 ± 1	–
ETV4$^{LPPL/QL}$	58 ± 4	42 ± 4	–
ETV4$^{LPPL/HL}$	53 ± 1	47 ± 1	–
ETV4$^{LPPL/QF}$	12 ± 1	34 ± 3	54 ± 3
ETV1$^{\Delta Nt}$	50 ± 7	50 ± 7	–
ETV4$^{\Delta Nt}$	4 ± 2	17 ± 4	79 ± 6

Discussion of Kinetic Data Analysis

The major strengths of the calculation method outlined above is that it is operationally simple, and that it performs very well when tested against simulated data in the relative rate

ranges we observed experimentally. Specifically, calculated values of microscopic rate constants obtained from simulated data were well within 20% of the input values, which is on the level of normal experimental error. However, we must note that this methodology performs poorly under conditions where $k_{R,2}$ approaches the value of $k_{R,1}$. In kinetic simulations, the range where this becomes problematic is when $k_{R,2} \geq 0.5 * k_{R,1}$; above this value of $k_{R,2}$ the equilibrium constant $K_{C,2}$ can be significantly underestimated. In the current study, this scenario only occurred for the variant ETV4$^{LPPL/QF}$ (see Tables S2 and S3), and this likely led to an underestimated $K_{C,2}$ value. Nonetheless, this variant was still detected by kinetic analysis as conformationally similar to wild-type ETV4, which is further supported by NMR analysis (see Fig. 3A in main text). As the value of $k_{R,2}$ increases beyond $k_{R,1}$ it becomes especially challenging to fit all three phases accurately, in this case because the amplitude of the corresponding kinetic phase shrinks considerably. This specific issue is not necessarily a drawback of our analysis approach, as other calculation methods and global fitting strategies cannot typically detect a fast step that follows a slow step. This type of kinetic behavior also may be why the some variants only have one observable conformational change. In the case where the second conformational change phase becomes undetectable due to an increase in $k_{R,2}$, the apparent population of C2 (as presented in the figures) would be the sum of the true populations of C2 and C3 conformers. We note that this possibility does not affect any of the conclusions presented in this work.

NMR Spectroscopy

Constant time $^{1}H,^{13}C$-HSQC experiments were performed with 50-75 μM uniformly $^{13}C,^{15}N$-labeled Med25 in NMR buffer (20 mM sodium phosphate pH 6.5, 150 mM NaCl, 3 mM DTT, 10% D_2O, and 2% DMSO) on a Bruker 600 MHz instrument equipped with a cryoprobe. HSQC experiments were processed in NMRPipe(3) and visualized with NMRFAM-Sparky.(4) All chemical shift perturbation analyses were performed on samples with 1.1 equivalents of unlabeled binding partner, which results in ≥96% bound Med25 based on measured K_d values. Peak assignments of PEA3-bound complexes were achieved by titration experiments with the unlabeled TAD with titration points of 0.2, 0.5, 0.8, and 1.1 equivalents of TAD, and assignments of mutations were made based on the parent TAD complexes. Native ETV1- and ETV4-bound spectra were representative of at least three biological replicates using different protein and

peptide stocks. Chemical shift perturbations (Δδ) were calculated from the proton ($\Delta\delta_H$) and carbon ($\Delta\delta_C$) chemical shifts by:

$$\Delta\delta = \sqrt{(\Delta\delta_H)^2 + (0.25 \times \Delta\delta_C)^2}$$

Assignments of side-chain methyl resonances of free Med25 were achieved through 3D H(CCCO)NH and (H)CC(CO)NH TOCSY experiments (23 ms TOCSY mixing time) performed with a sample of 600 μM $^{13}C,^{15}N$ Med25 on a Bruker 800 MHz instrument equipped with a cryoprobe. An additional non-uniformly sampled 4D HCC(CO)NH TOCSY experiment(5) (12 ms TOCSY mixing time and 25% sampling) with a sample of 400 μM $^{13}C,^{15}N$ Med25 was performed to supplement the 3D experiments. $^{1}H,^{13}C$ resonance assignment from these experiments was enabled by a previous assignment of the Med25 $^{1}H,^{15}N$-HSQC spectrum,(1) however of 141 possible assignable non-proline amide resonances only 117 had been assigned, which precluded full assignment of the methyl spectrum. Thus, a supplemental set of TROSY-based HNCACB and CBCA(CO)NH experiments were performed to enable more complete assignment of $^{1}H,^{15}N$ resonances using a 600 μM sample of $^{13}C,^{15}N$ Med25 on a Bruker 800 MHz instrument. From these experiments, 132 of 141 amide resonances along with 83 of 89 methyl resonances were assigned. Unassigned methyl resonances include one diastereotopic methyl of Leu399 and both methyls of Leu544, the latter of which is a cloning artifact and not part of the native Med25 sequence. Three residues, Leu427, Ile453, and Ile526 are not possible to assign from the TOCSY experiments as they are directly before Pro residues in the primary sequence. However, at least one methyl from each of these residues were previously assigned by another group(6) and were well separated from other resonances. The full $^{1}H,^{13}C$-HSQC spectral assignment is shown below (Fig. S3) along with a structural representation of the assignment (Fig. S4).

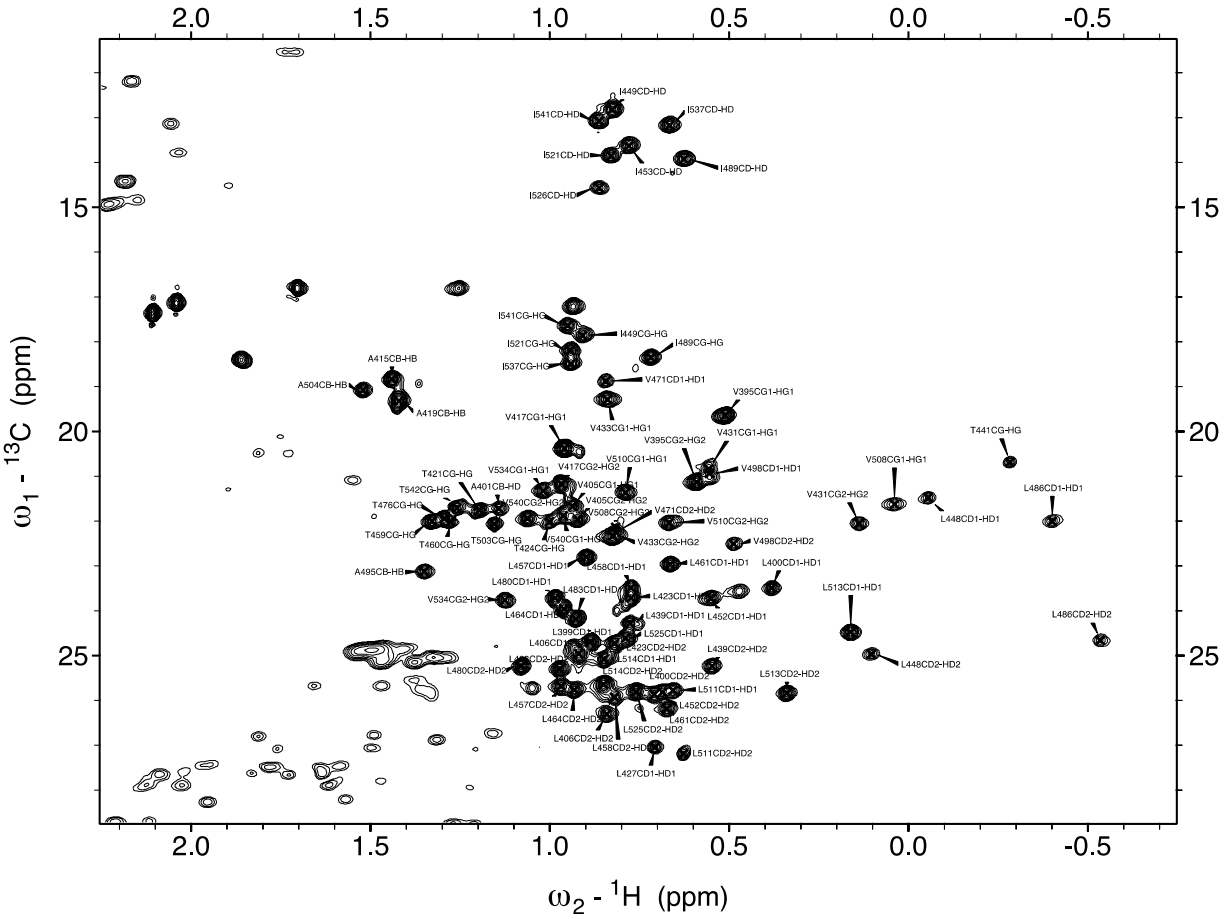

Figure S3. Assigned methyl $^{1}H,^{13}C$-HSQC spectrum of Med25. Experiment was conducted at 600 μM Med25 and 800 MHz field strength.

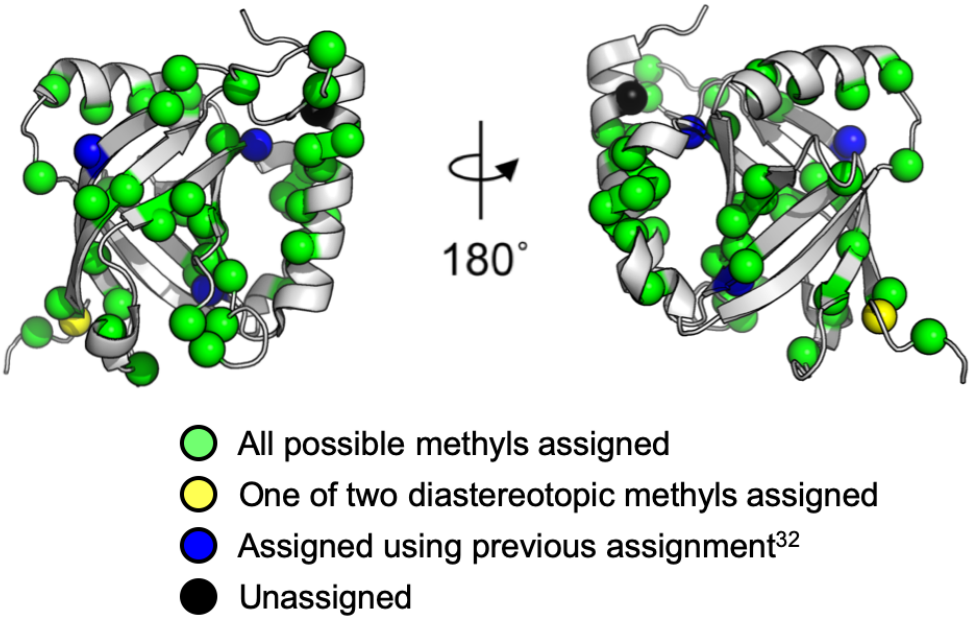

Figure S4. Assigned residues with methyl groups plotted on structure of Med25 (PDB ID 2XNF).(7) Green: all possible methyl groups for the residue were assigned using either the two 3D HCC(CO)NH TOCSY experiments, or the HNCACB experiment (for remaining Ala residues before Pro in the sequence). Yellow: only one of two diastereotopic methyls were assigned from the TOCSY experiments. Blue: well-dispersed methyls for the residue were assigned using a previous methyl assignment.*(6)* In all cases, these residues were before Pro residues in the sequence and thus were not observed in the HCC(CO)NH TOCSY experiments. Black: unassigned.

Kinetic Data

The full kinetic datasets used to generate the figures in the manuscript are shown below

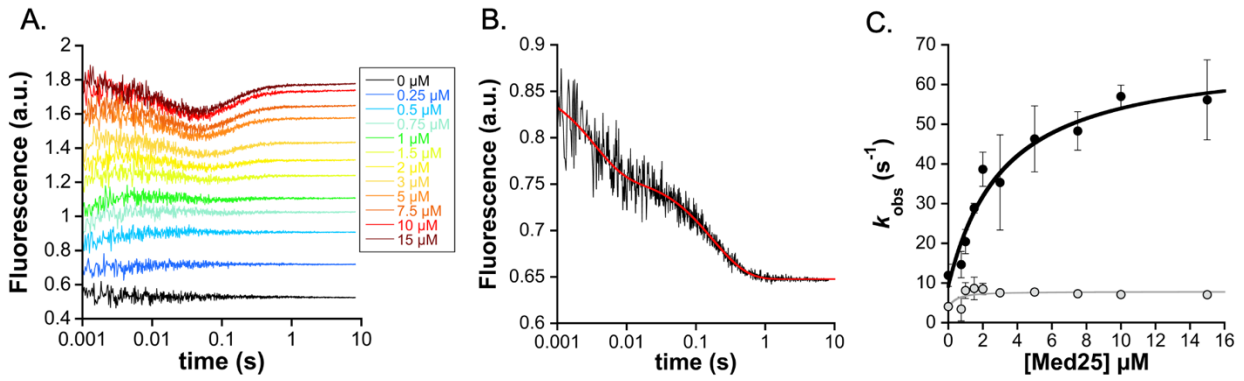

Figure S5. A. Association traces for binding of 0.25 μM 4-DMN-ETV1(38-69) to Med25. Concentrations of Med25 are as noted. B. Dissociation trace from 0.25 μM 4-DMN-ETV1(38-69) prebound to 0.5 μM Med25, mixed with 50 μM unlabeled ETV1(38-69). C. Observed rate constants for conformational change phases from curve fitting (black=fast phase, grey=slow phase). Values are average of *n*=3 biological replicates, and error represents the standard deviation.

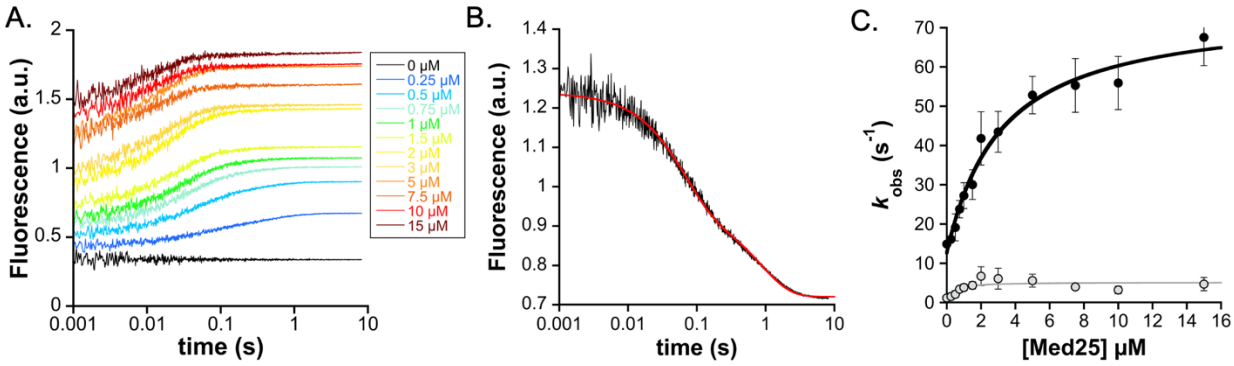

Figure S6. A. Association traces for binding of 0.25 μM 4-DMN-ETV4(45-76) to Med25. Concentrations of Med25 are as noted. B. Dissociation trace from 0.25 μM 4-DMN-ETV4(45-76) prebound to 0.5 μM Med25, mixed with 50 μM unlabeled ETV4(45-76). C. Observed rate constants for conformational change phases from curve fitting (black=fast phase, grey=slow phase). Values are average of *n*=4 biological replicates, and error represents the standard deviation.

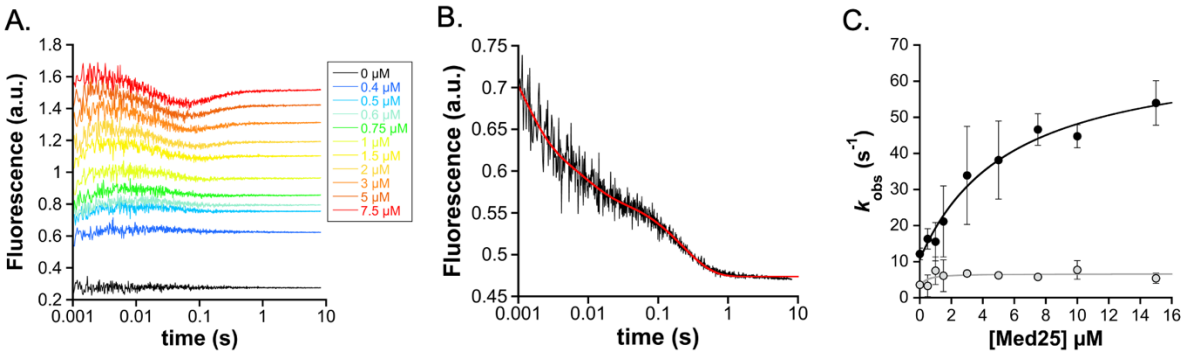

Figure S7. A. Association traces for binding of 0.25 μM 4-DMN-ETV5(38-68) to Med25. Concentrations of Med25 are as noted. B. Dissociation trace from 0.25 μM 4-DMN-ETV5(38-68) prebound to 0.5 μM Med25, mixed with 50 μM unlabeled ETV5(38-68). C. Observed rate constants for conformational change phases from curve fitting (black=fast phase, grey=slow phase). Values are average of *n*=3 biological replicates, and error represents the standard deviation.

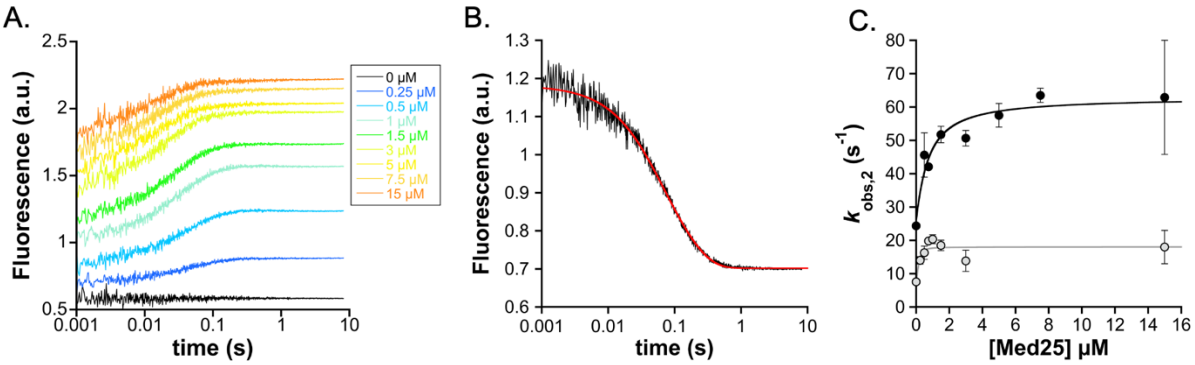

Figure S8. A. Association traces for binding of 0.25 μM 4-DMN-ETV4(45-76)^{QF} to Med25. Concentrations of Med25 are as noted. B. Dissociation trace from 0.25 μM 4-DMN-ETV4(45-76)^{QF} prebound to 0.5 μM Med25, mixed with 50 μM unlabeled ETV4(45-76). C. Observed rate constants for conformational change phases from curve fitting (black=fast phase, grey=slow phase). Values are average of *n*=2 biological replicates, and error represents the standard deviation.

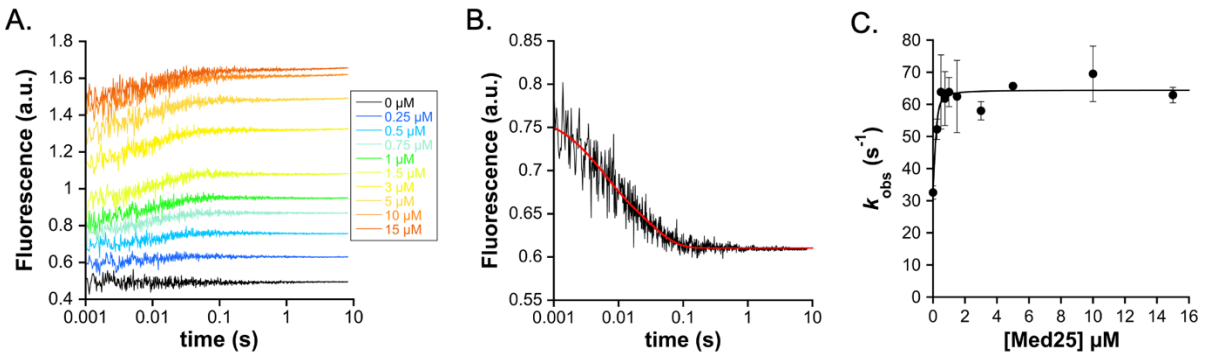

Figure S9. A. Association traces for binding of 0.25 μM 4-DMN-ETV4(45-76)^{QL} to Med25. Concentrations of Med25 are as noted. B. Dissociation trace from 0.25 μM 4-DMN-ETV4(45-76)^{QL} prebound to 0.5 μM Med25, mixed with 50 μM unlabeled ETV4(45-76). C. Observed rate constants for conformational change phases from curve fitting (black=fast phase, grey=slow phase). Values are average of *n*=2 biological replicates, and error represents the standard deviation.

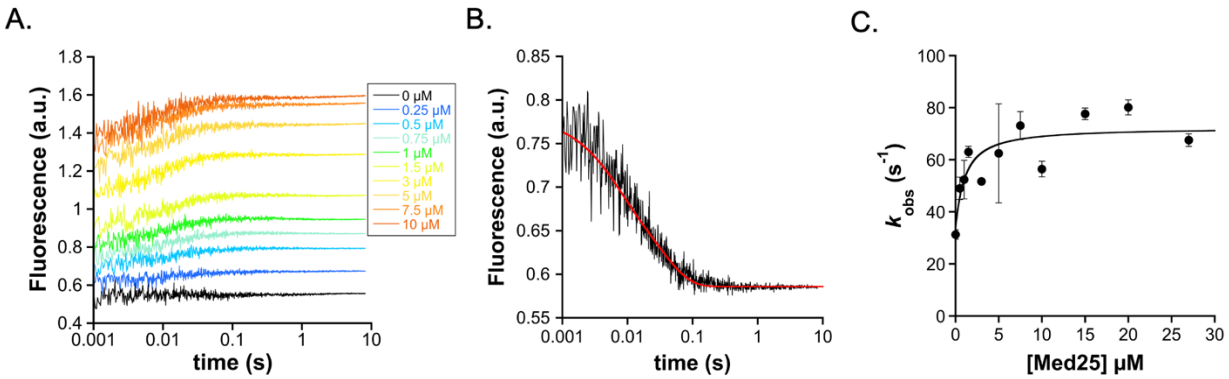

Figure S10. A. Association traces for binding of 0.25 μM 4-DMN-ETV4(45-76)^{HL} to Med25. Concentrations of Med25 are as noted. B. Dissociation trace from 0.25 μM 4-DMN-ETV4(45-76)^{HL} prebound to 0.5 μM Med25, mixed with 50 μM unlabeled ETV4(45-76). C. Observed rate constants for conformational change phases from curve fitting (black=fast phase, grey=slow phase). Values are average of *n*=2 biological replicates, and error represents the standard deviation.

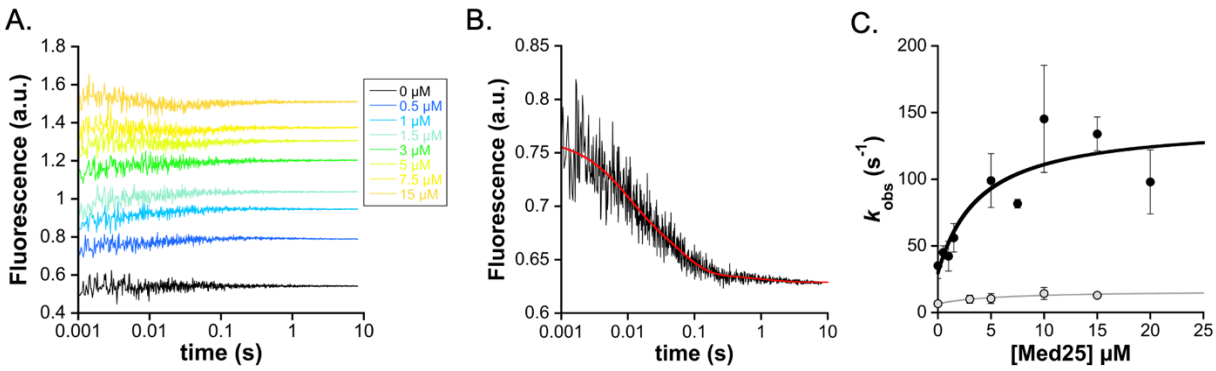

Figure S11. A. Association traces for binding of 0.25 μM 4-DMN-ETV4(45-76)$^{DLAH/HL}$ to Med25. Concentrations of Med25 are as noted. B. Dissociation trace from 0.25 μM 4-DMN-ETV4(45-76)$^{DLAH/HL}$ prebound to 0.5 μM Med25, mixed with 50 μM unlabeled ETV4(45-76). C. Observed rate constants for conformational change phases from curve fitting (black=fast phase, grey=slow phase). Values are average of *n*=2 biological replicates, and error represents the standard deviation.

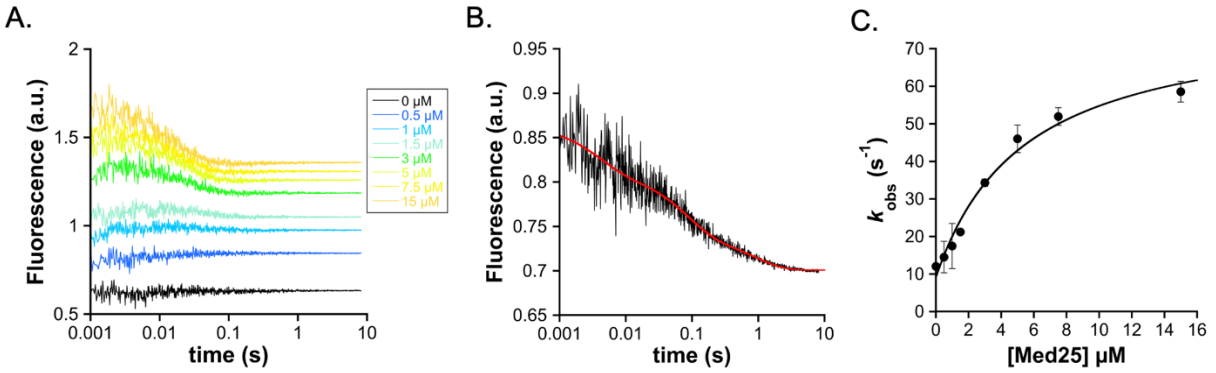

Figure S12. A. Association traces for binding of 0.25 μM 4-DMN-ETV4(45-76)$^{DLAH/HF}$ to Med25. Concentrations of Med25 are as noted. B. Dissociation trace from 0.25 μM 4-DMN-ETV4(45-76)$^{DLAH/HF}$ prebound to 0.5 μM Med25, mixed with 50 μM unlabeled ETV4(45-76). C. Observed rate constants for conformational change phases from curve fitting (black=fast phase, grey=slow phase). Values are average of *n*=2 biological replicates, and error represents the standard deviation.

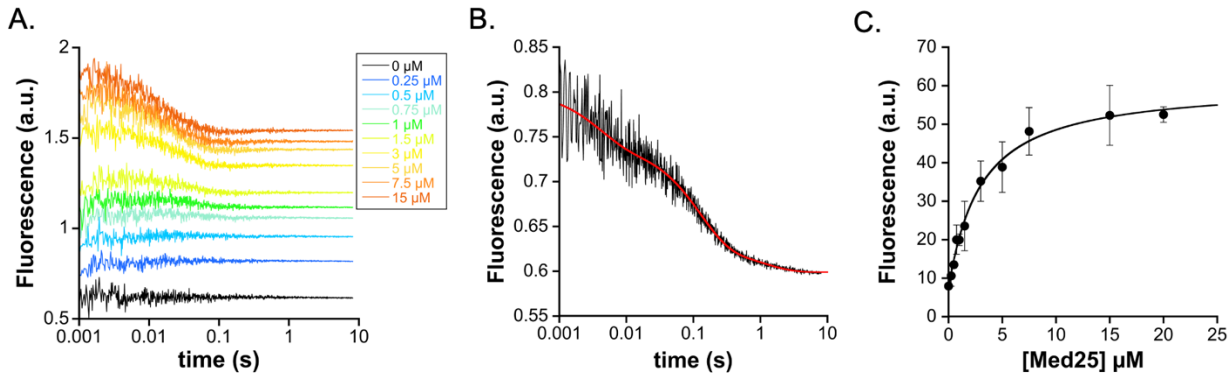

Figure S13. A. Association traces for binding of 0.25 μM 4-DMN-ETV4(45-76)$^{DLAH/QF}$ to Med25. Concentrations of Med25 are as noted. B. Dissociation trace from 0.25 μM 4-DMN-ETV4(45-76)$^{DLAH/QF}$ prebound to 0.5 μM Med25, mixed with 50 μM unlabeled ETV4(45-76). C. Observed rate constants for conformational change phases from curve fitting (black=fast phase, grey=slow phase). Values are average of *n*=2 biological replicates, and error represents the standard deviation.

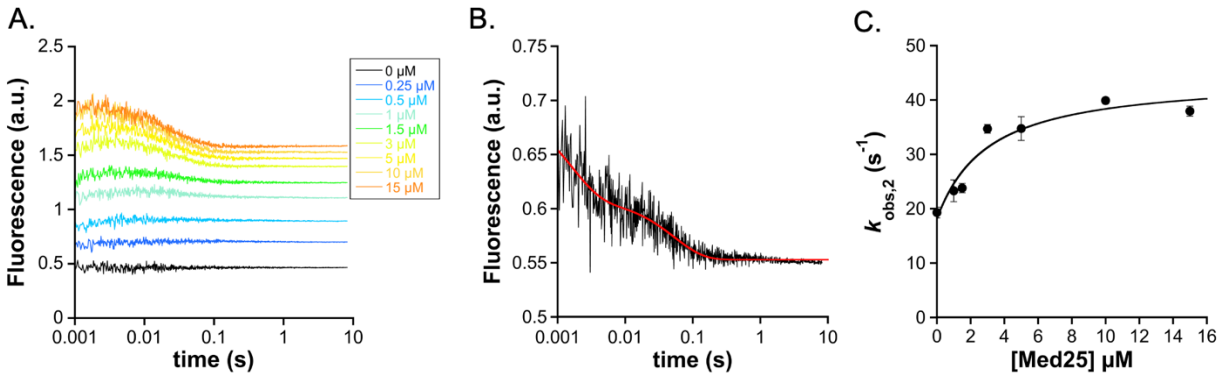

Figure S14. A. Association traces for binding of 0.25 μM 4-DMN-ETV1(42-69) to Med25. Concentrations of Med25 are as noted. B. Dissociation trace from 0.25 μM 4-DMN-ETV1(42-69) prebound to 0.5 μM Med25, mixed with 50 μM unlabeled ETV1(38-69). C. Observed rate constants for conformational change phases from curve fitting (black=fast phase, grey=slow phase). Values are average of *n*=2 biological replicates, and error represents the standard deviation.

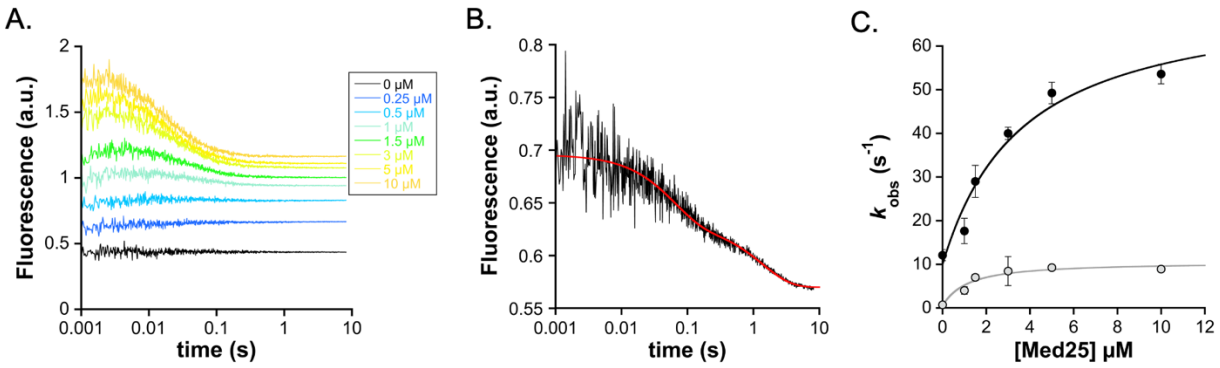

Figure S15. A. Association traces for binding of 0.25 μM 4-DMN-ETV4(49-76) to Med25. Concentrations of Med25 are as noted. B. Dissociation trace from 0.25 μM 4-DMN-ETV4(49-76) prebound to 0.5 μM Med25, mixed with 50 μM unlabeled ETV4(45-76). C. Observed rate constants for conformational change phases from curve fitting (black=fast phase, grey=slow phase). Values are average of *n*=2 biological replicates, and error represents the standard deviation.

NMR Data

The full NMR datasets used to generate the figures in the manuscript are shown below.

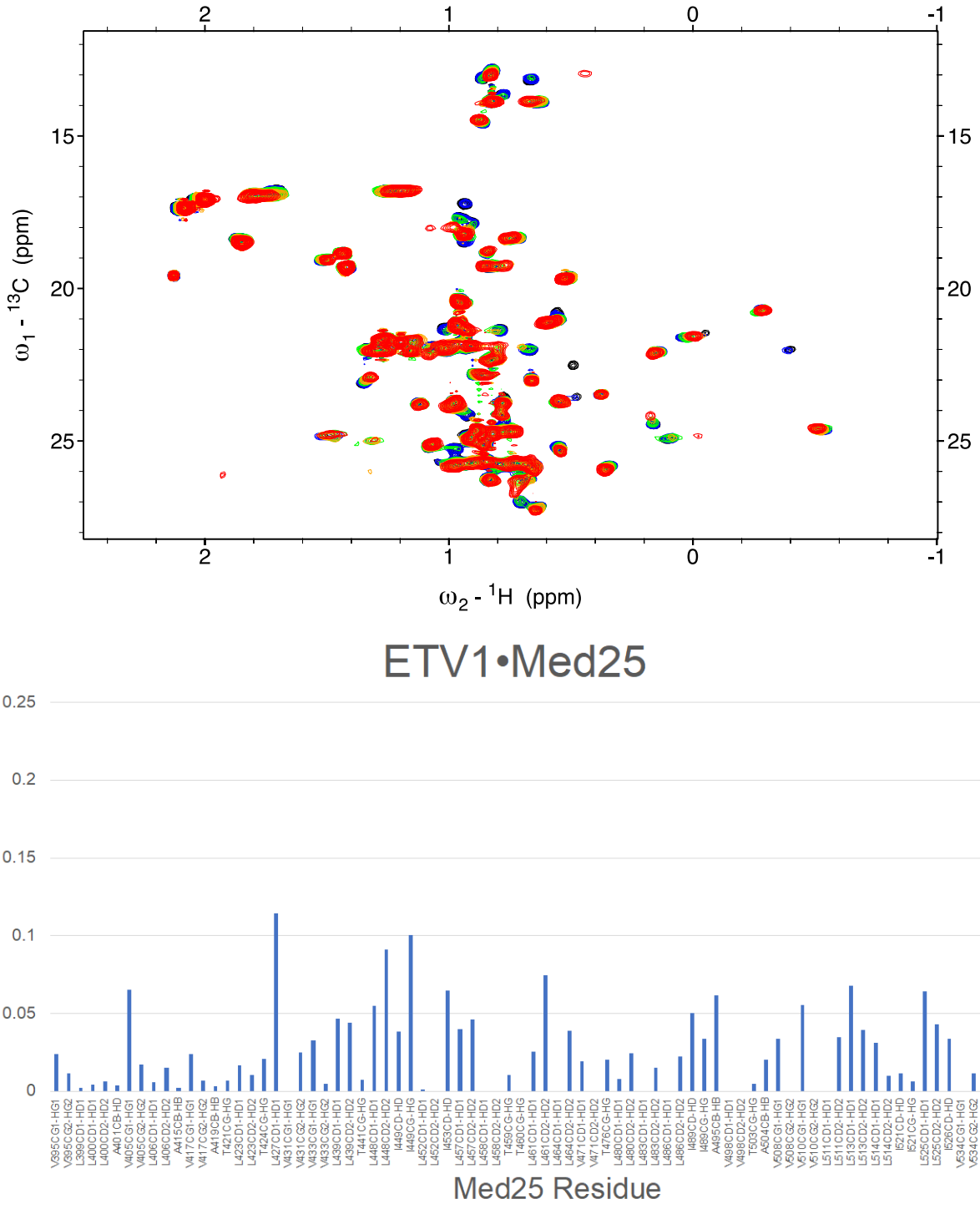

Figure S16. Above: Overlay of $^{1}H,^{13}C$ HSQC spectra of Med25 upon titration with unlabeled ETV1. Spectra are free Med25 (50 μM, black), 0.2 eq ETV1 (blue), 0.5 eq ETV1 (green), 0.8 eq ETV1 (orange) 1.1 eq ETV1 (red). Below: CSP mapping of Med25 bound to 1.1 eq ETV1.

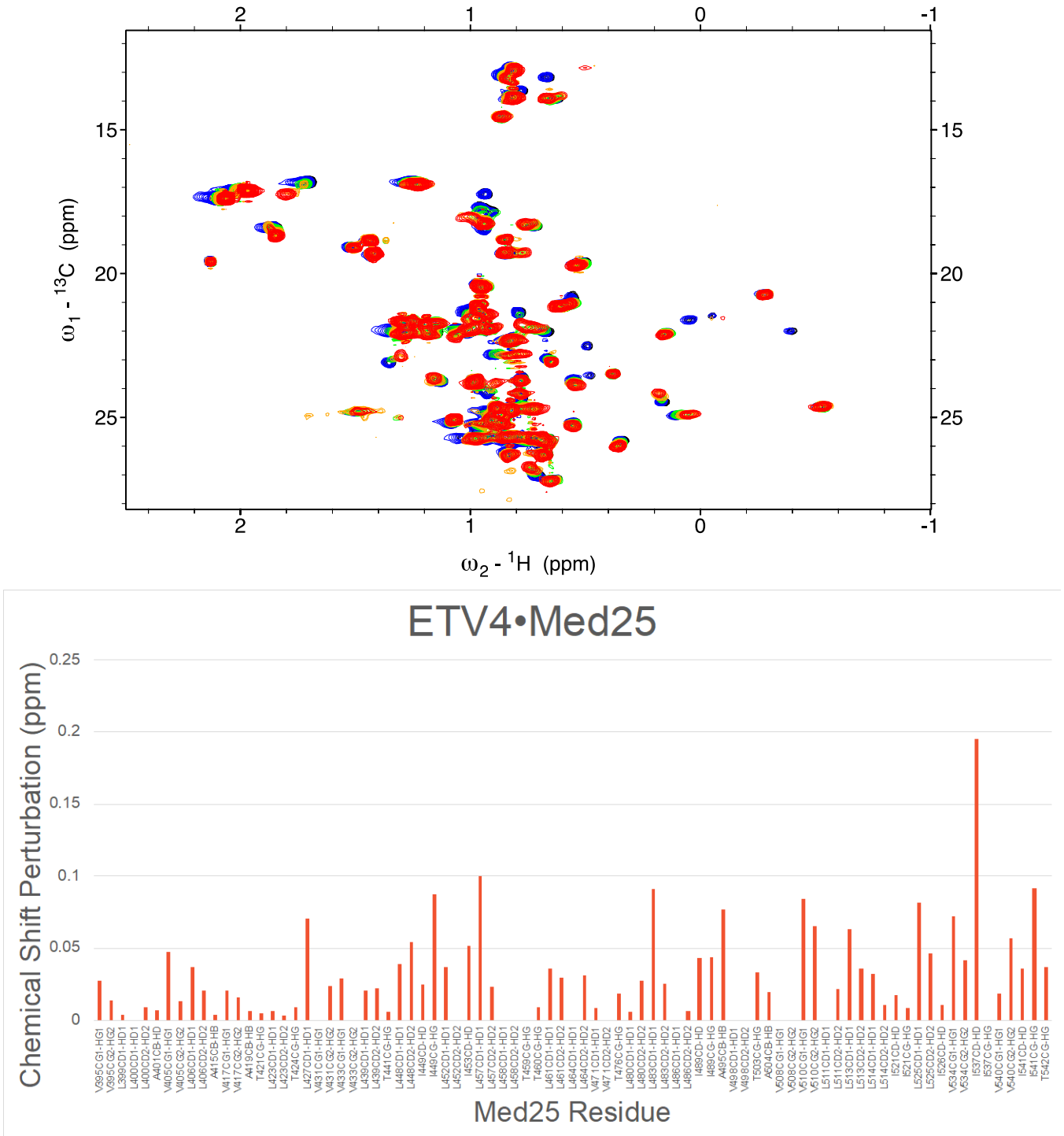

Figure S17. Above: Overlay of ^{1}H,^{13}C HSQC spectra of Med25 upon titration with unlabeled ETV4. Spectra are free Med25 (50 μM, black), 0.2 eq ETV4 (blue), 0.5 eq ETV4 (green), 0.8 eq ETV4 (orange) 1.1 eq ETV4 (red). Below: CSP mapping of Med25 bound to 1.1 eq ETV4.

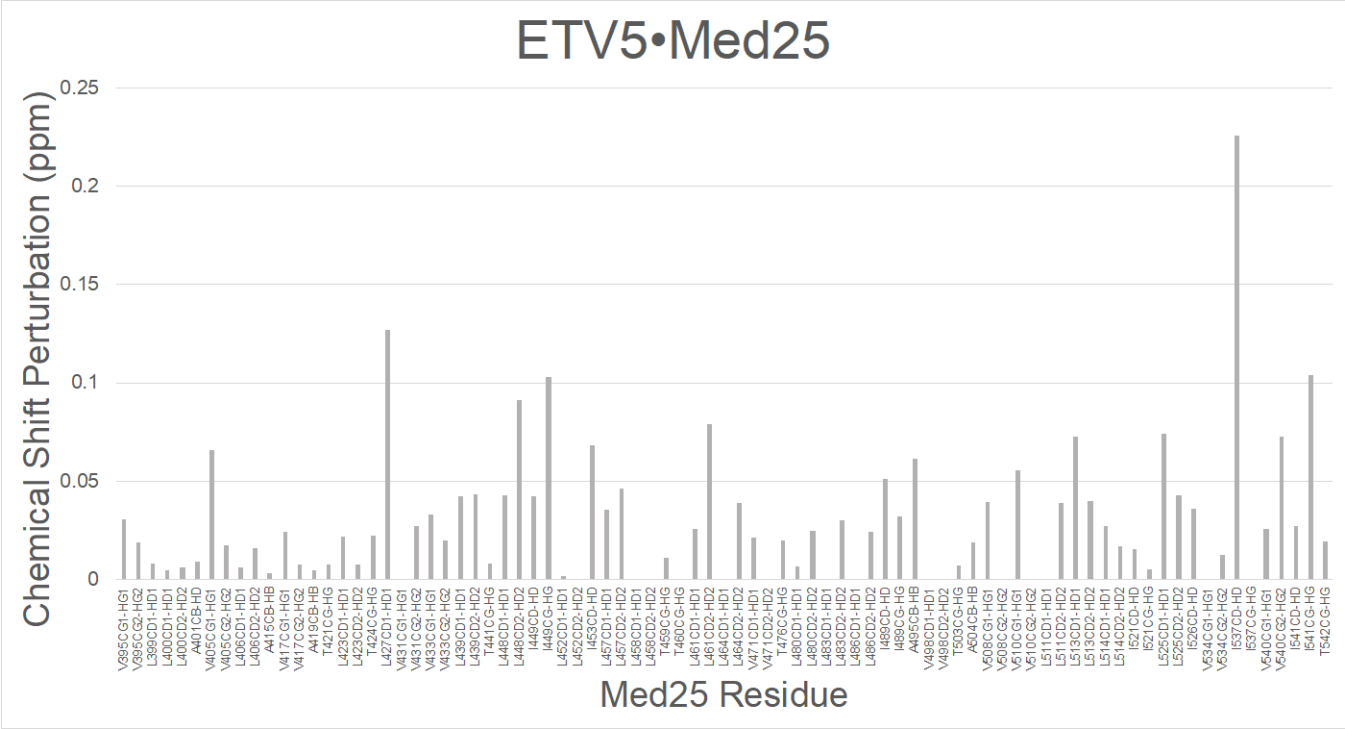

Figure S18. CSP mapping of Med25 bound to 1.1 eq ETV5. Assignments were generated by comparison to the essentially identical spectra of Med25 bound to ETV1.

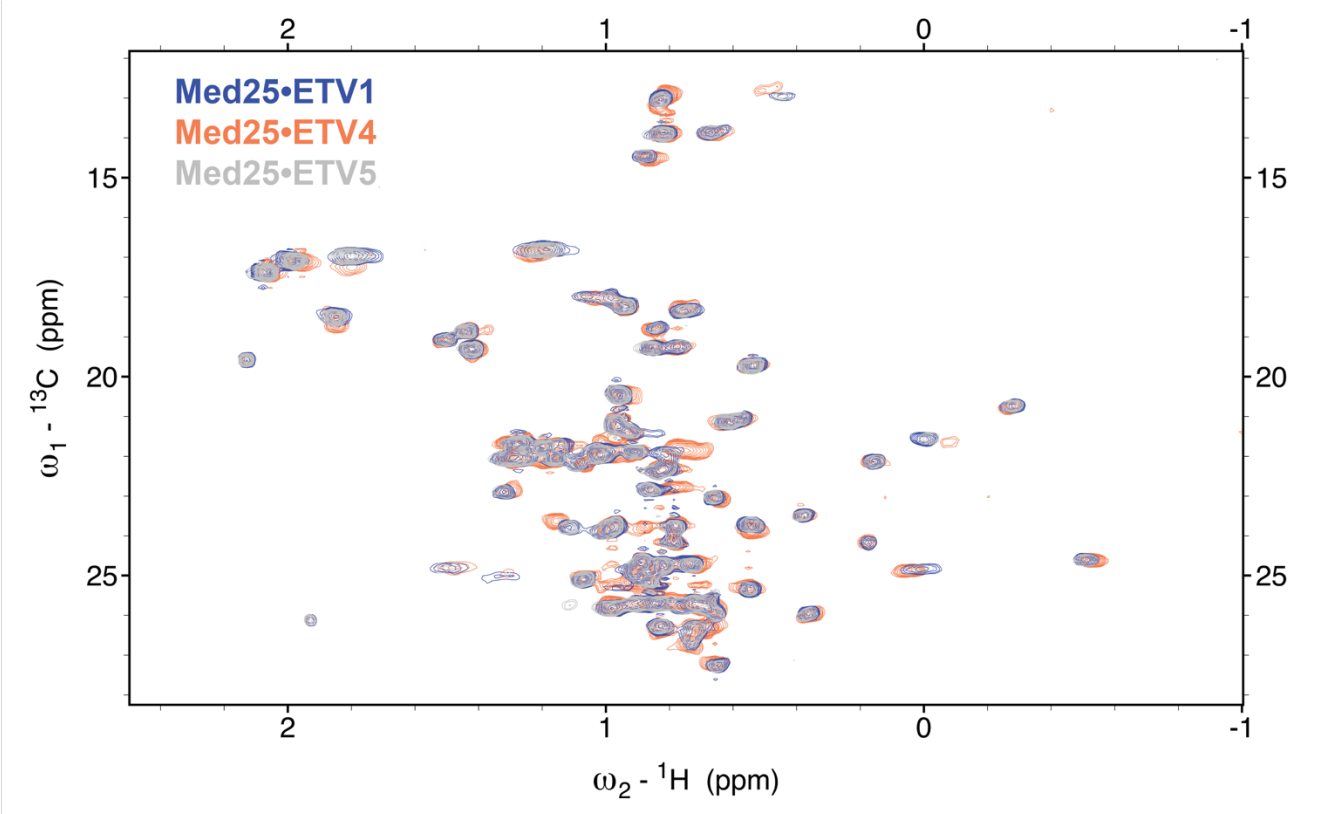

Figure S19. Overlay of ^{1}H,^{13}C HSQC spectra of Med25 bound to ETV1 (blue), ETV4 (orange), and ETV5 (grey).

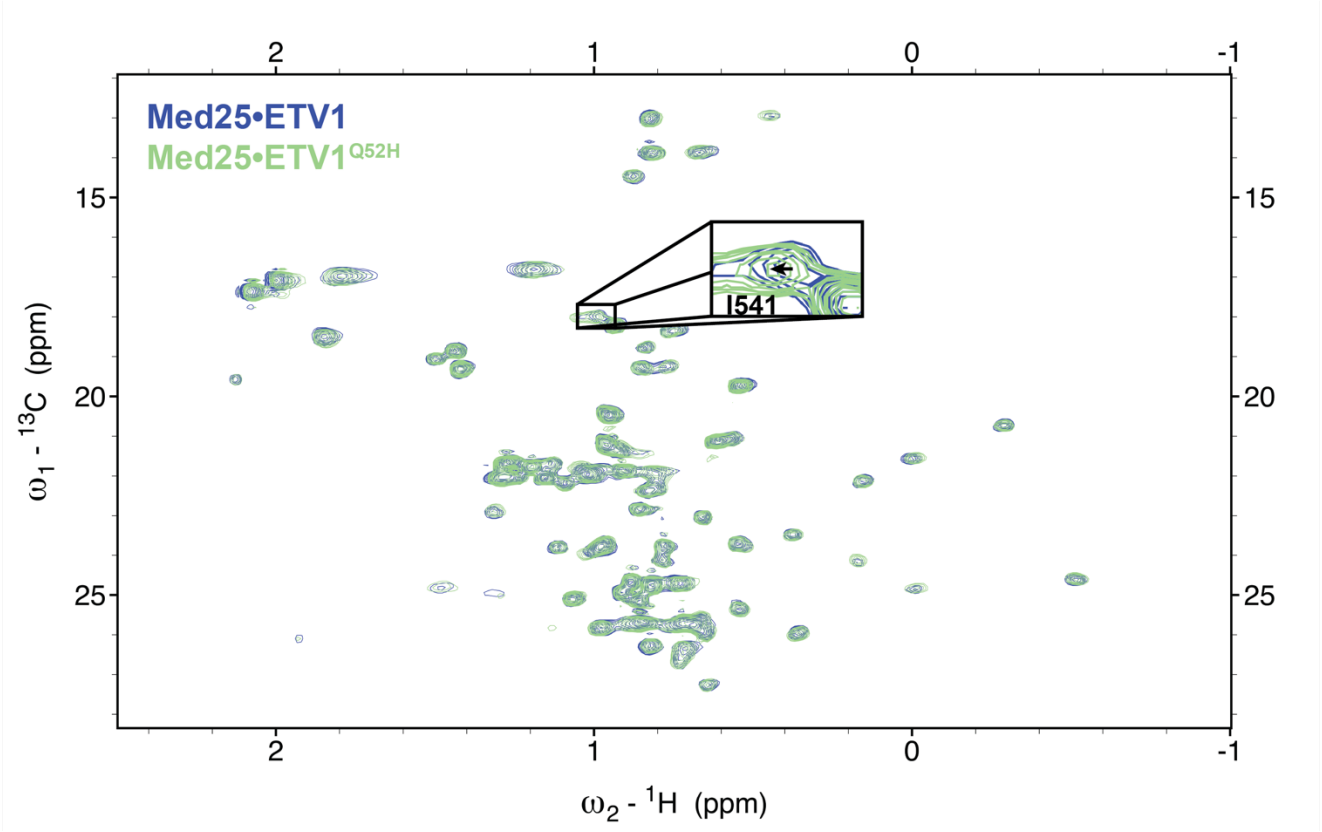

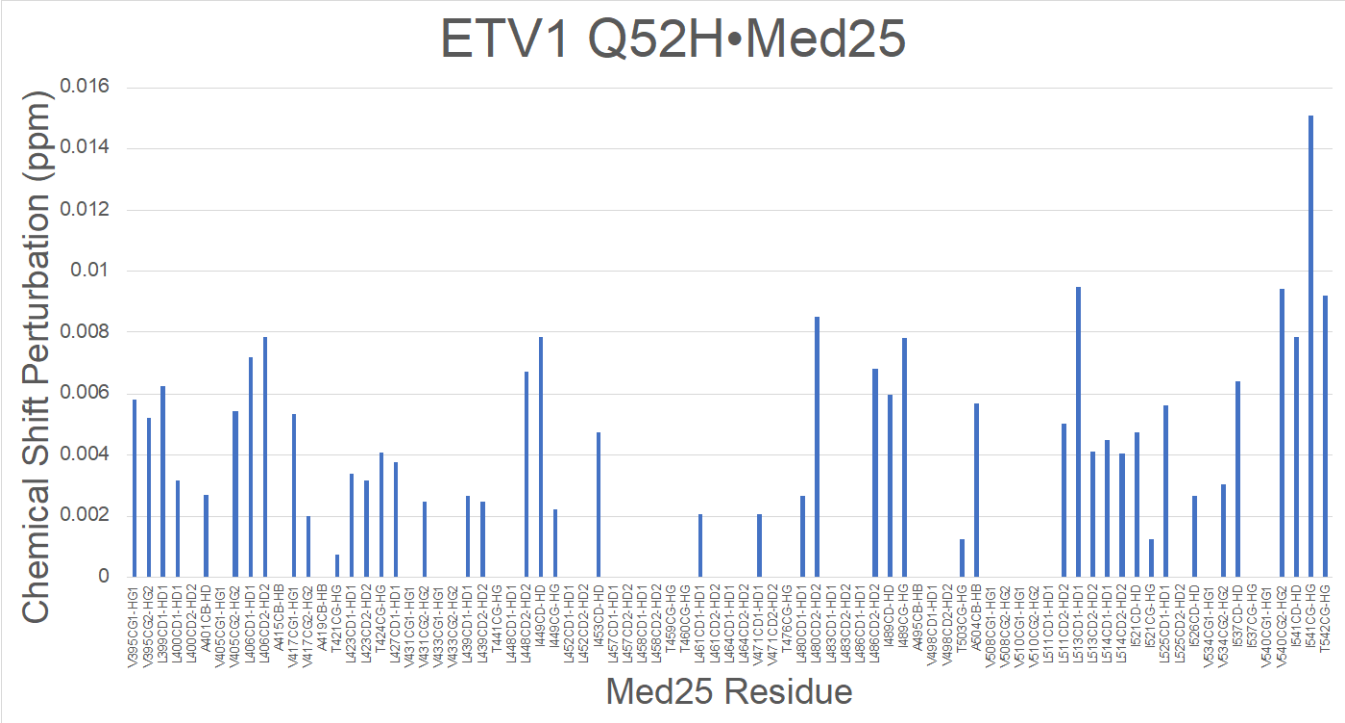

Figure S20. Above: Overlay of $^{1}H,^{13}C$ HSQC spectra of Med25 bound to ETV1 helical region soft mutation variant. Spectra are Med25 (60 μM) bound to 1.1 eq ETV1 (blue) or ETV1^{Q52H} (green). Below: CSP mapping of differences between ETV1- and ETV1^{Q52H}-bound Med25 spectra.

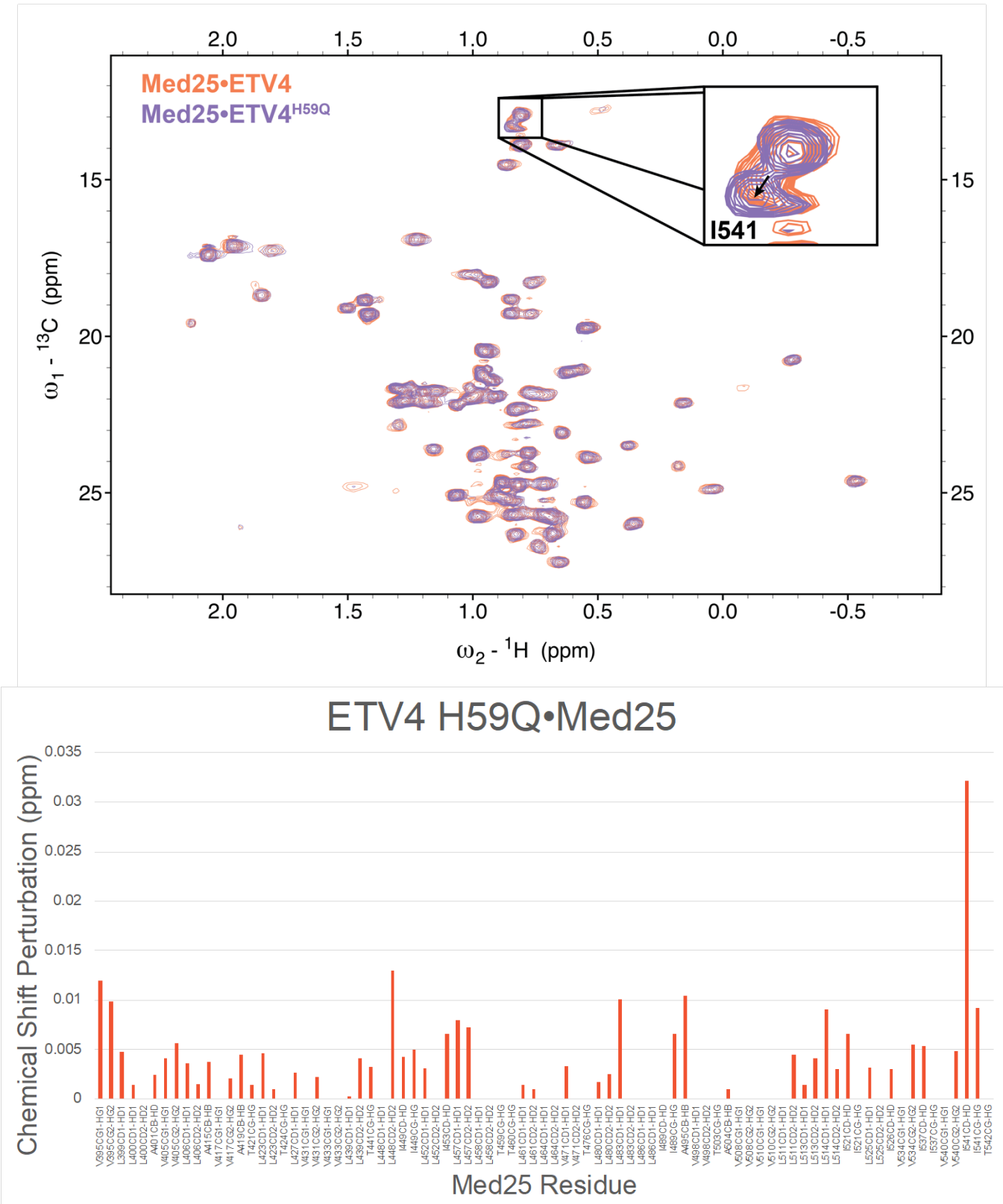

Figure S21. Above: Overlay of $^{1}H,^{13}C$ HSQC spectra of Med25 bound to ETV4 helical region soft mutation variant. Spectra are Med25 (60 μM) bound to 1.1 eq ETV4 (orange) or ETV4^{H59Q} (light purple). Below: CSP mapping of differences between ETV4- and ETV4^{H59Q}-bound Med25 spectra.

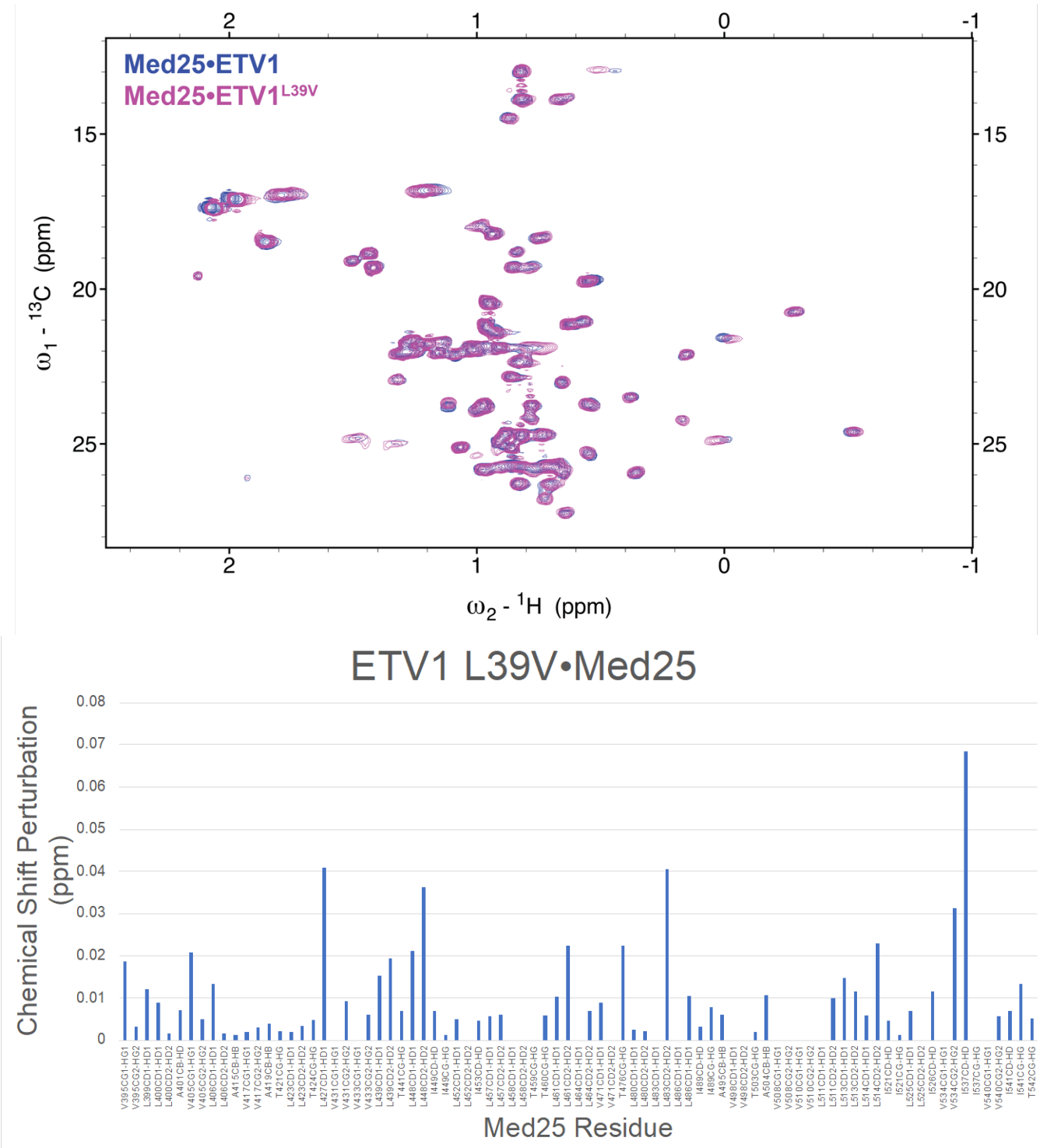

Figure S22. Above: Overlay of $^{1}H,^{13}C$ HSQC spectra of Med25 bound to ETV1 *N*-terminal soft mutation variant. Spectra are Med25 (70 μM) bound to 1.1 eq ETV1 (blue) or ETV1^{L39V} (purple). Below: CSP mapping of differences between ETV1- and ETV1^{L39V}-bound Med25 spectra.

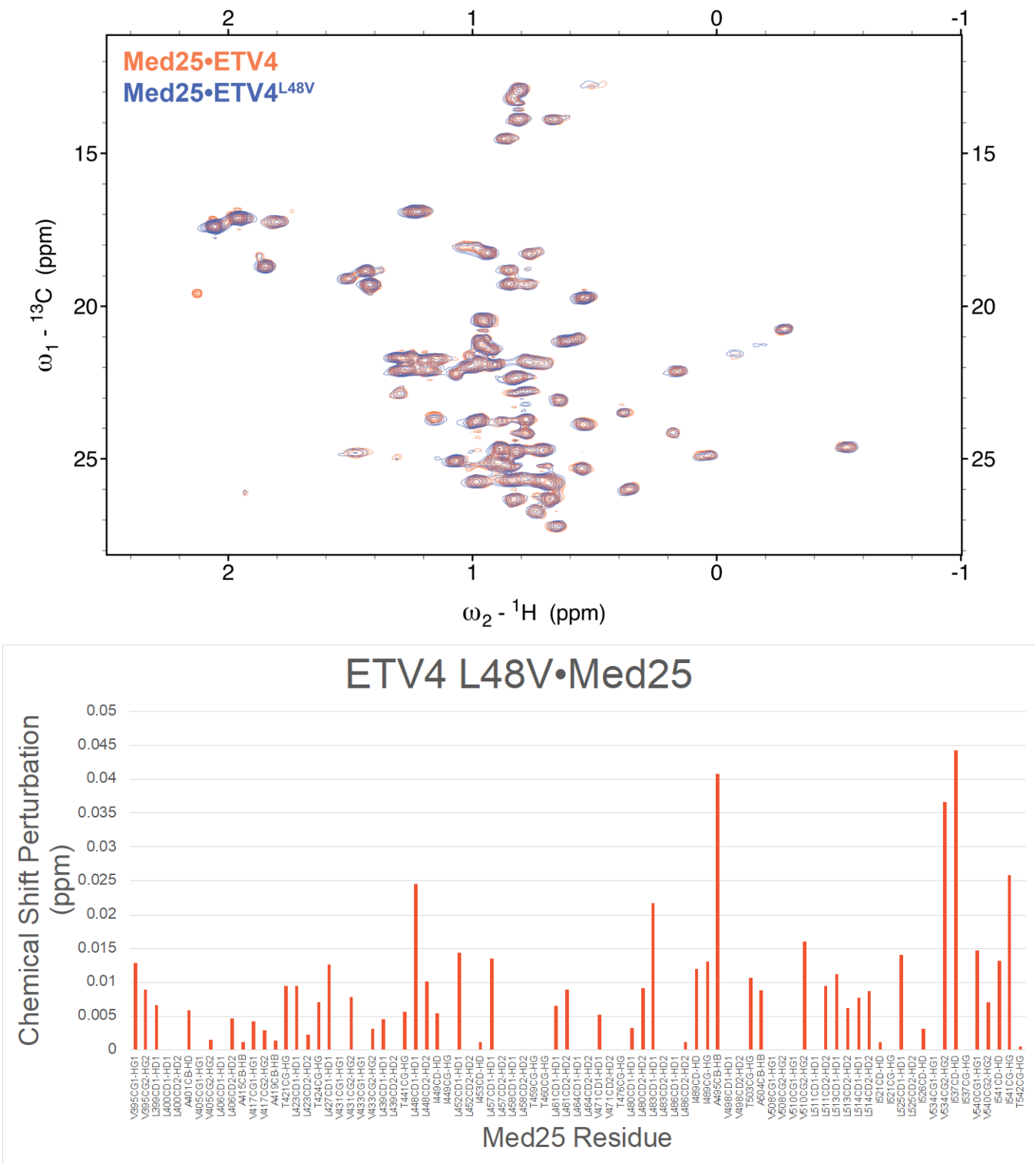

Figure S23. Above: Overlay of $^{1}H,^{13}C$ HSQC spectra of Med25 bound to ETV4 *N*-terminal soft mutation variant. Spectra are Med25 (70 μM) bound to 1.1 eq ETV4 (orange) or ETV4^{L48V} (blue). Below: CSP mapping of differences between ETV4- and ETV4^{L48V}-bound Med25 spectra.

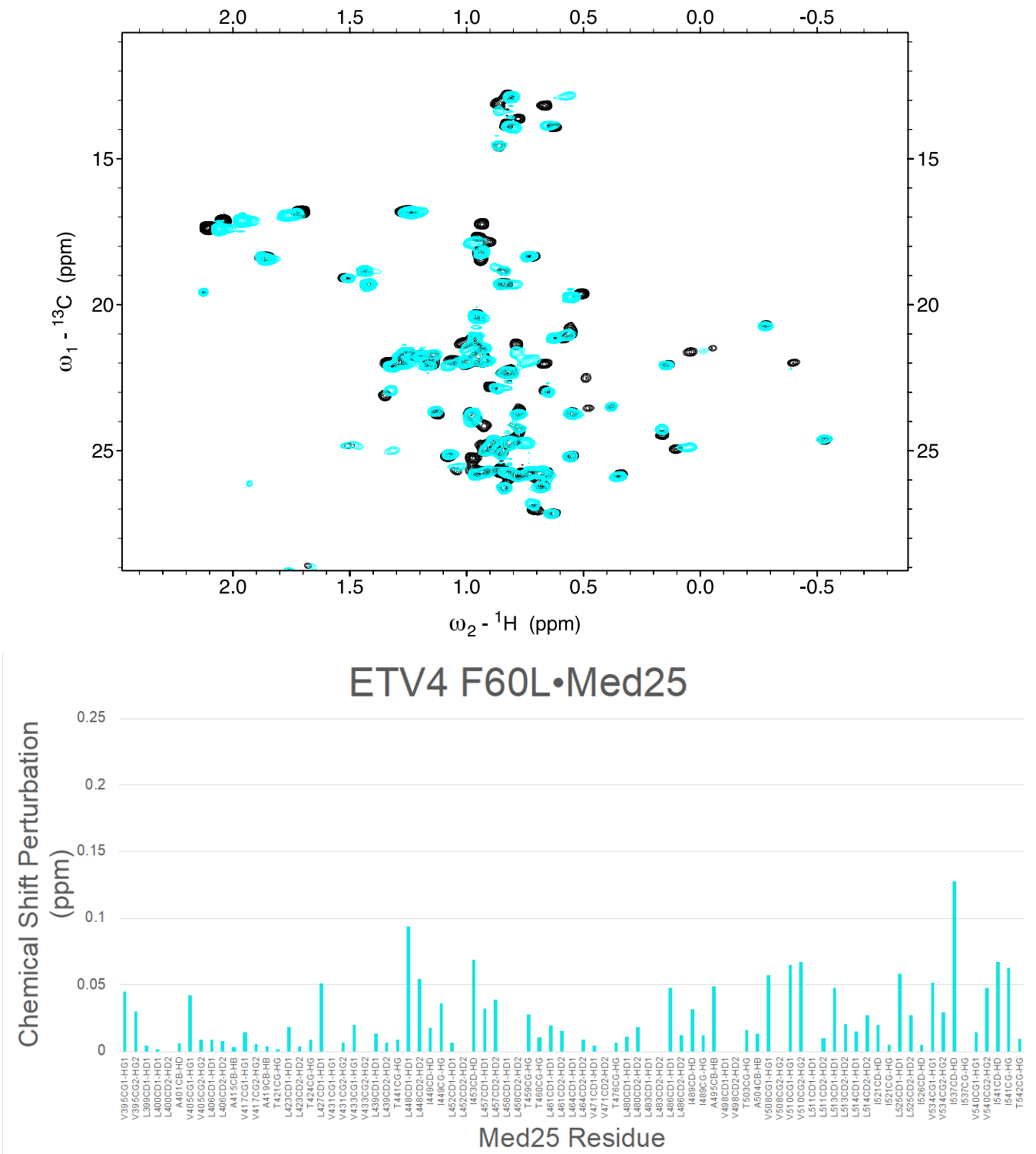

Figure S24. Above: Overlay of $^{1}H,^{13}C$ HSQC spectra of Med25 bound to ETV4 helical region variant that redistributes conformational ensemble. Spectra are Med25 (60 μM, black) and Med25 bound to 1.1 eq ETV4^{F60L} (cyan). Below: CSP mapping of Med25 bound to ETV4^{F60L}.

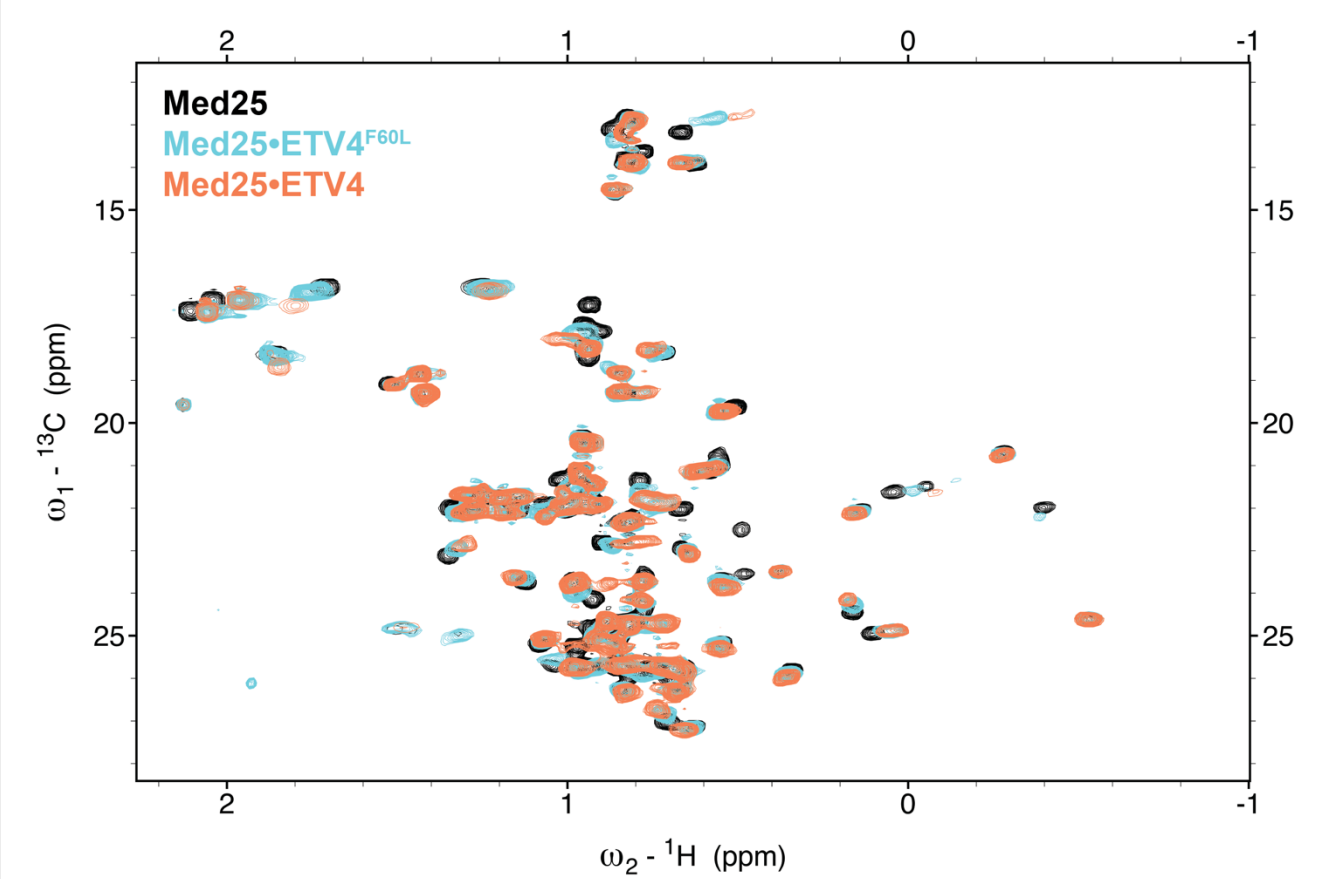

Figure S25. Overlay of $^{1}H,^{13}C$ HSQC spectra of free Med25 (60 μM, black), 1.1 eq ETV4^{F60L} (cyan), 1.1 eq ETV4 (orange).

Peptide Characterization

The characterization data for all peptides in this manuscript is shown below.

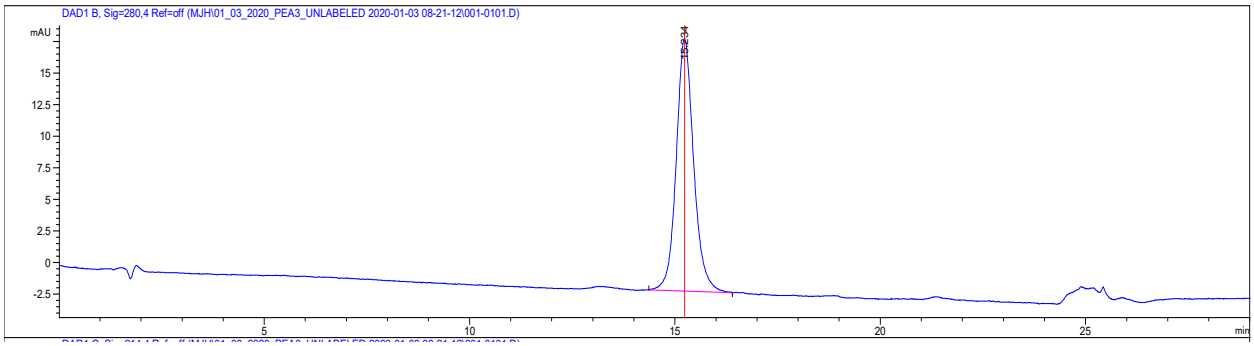

Analytical HPLC trace of **ETV1(38-69)**, monitored at 280 nm. Analytical sample was run in a water (with 100 mM ammonium acetate)/ acetonitrile system. The sample was injected with an isocratic flow of 70% water (with 100 mM ammonium acetate) and 30% acetonitrile. After 2 min, the solvent gradient was increased from 10-35% acetonitrile over 20 min.

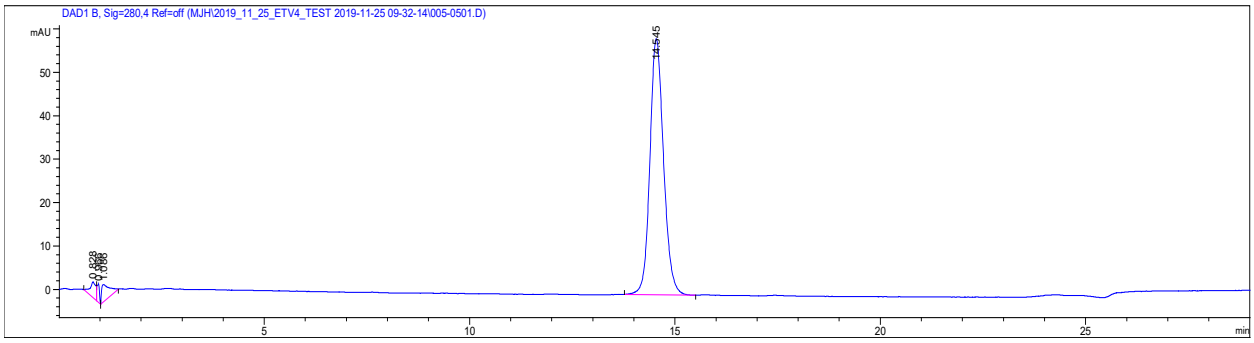

Analytical HPLC trace of **ETV4(45-76)**, monitored at 280 nm. Analytical sample was run in a water (with 100 mM ammonium acetate)/ acetonitrile system. The sample was injected with an isocratic flow of 70% water (with 100 mM ammonium acetate) and 30% acetonitrile. After 2 min, the solvent gradient was increased from 10-35% acetonitrile over 20 min.

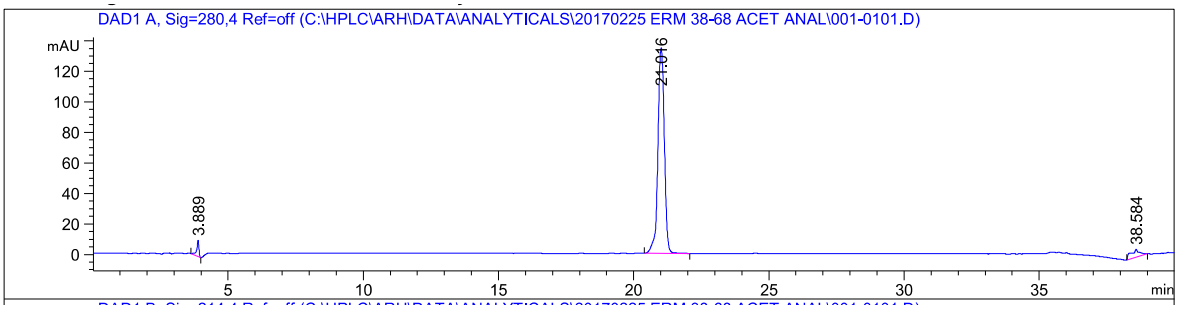

Analytical HPLC trace of **ETV5(38-68)**, monitored at 280 nm. Analytical sample was run in a water (with 100 mM ammonium acetate)/acetonitrile system. The sample was injected with an isocratic flow of 85% water (with 100 mM ammonium acetate) and 15% acetonitriile. After 2 min, the solvent gradient was increased from 15-30% acetonitrile over 20 min.

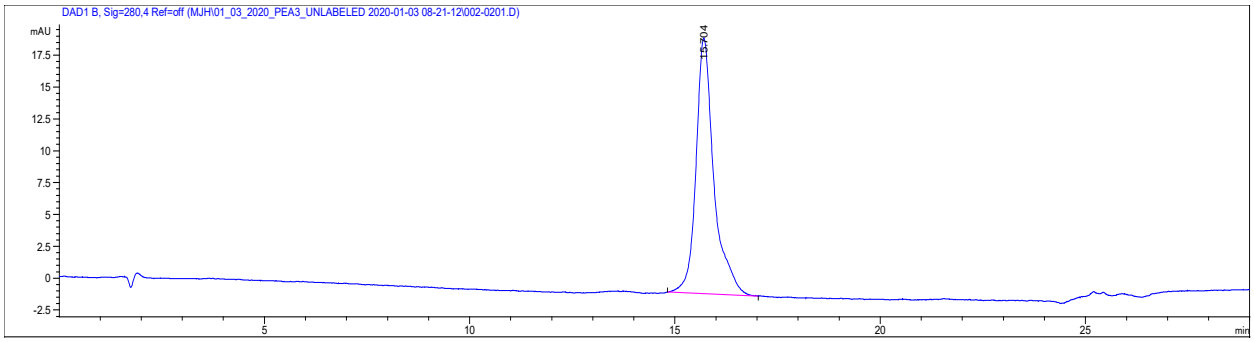

Analytical HPLC trace of **ETV1(38-69)^{Q52H}**, monitored at 280 nm. Analytical sample was run in a water (with 100 mM ammonium acetate)/ acetonitrile system. The sample was injected with an isocratic flow of 70% water (with 100 mM ammonium acetate) and 30% acetonitrile. After 2 min, the solvent gradient was increased from 10-35% acetonitrile over 20 min.

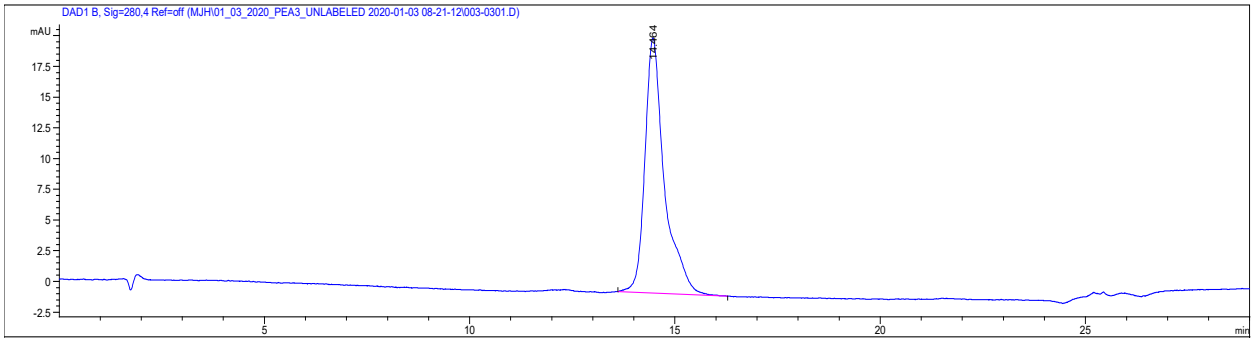

Analytical HPLC trace of **ETV1(38-69)^{L39V}**, monitored at 280 nm. Analytical sample was run in a water (with 100 mM ammonium acetate)/ acetonitrile system. The sample was injected with an isocratic flow of 70% water (with 100 mM ammonium acetate) and 30% acetonitrile. After 2 min, the solvent gradient was increased from 10-35% acetonitrile over 20 min.

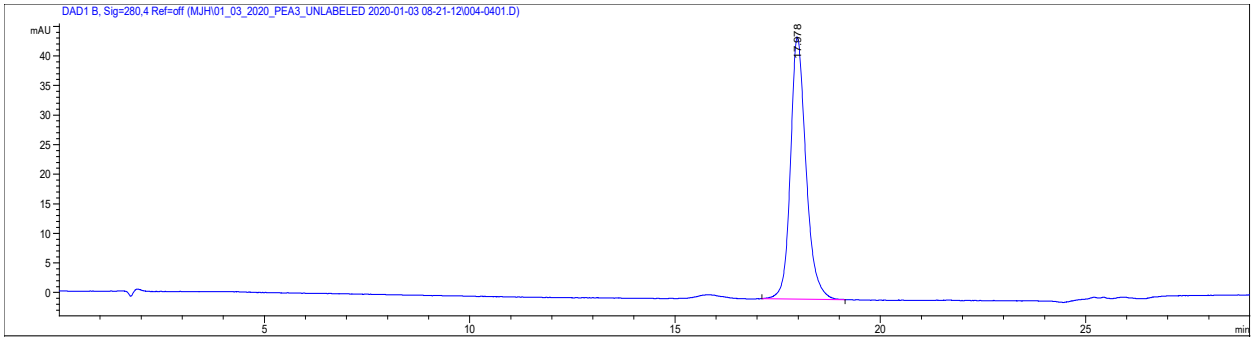

Analytical HPLC trace of **ETV4(45-76)^{F60L}**, monitored at 280 nm. Analytical sample was run in a water (with 100 mM ammonium acetate)/ acetonitrile system. The sample was injected with an isocratic flow of 70% water (with 100 mM ammonium acetate) and 30% acetonitrile. After 2 min, the solvent gradient was increased from 10-35% acetonitrile over 20 min.

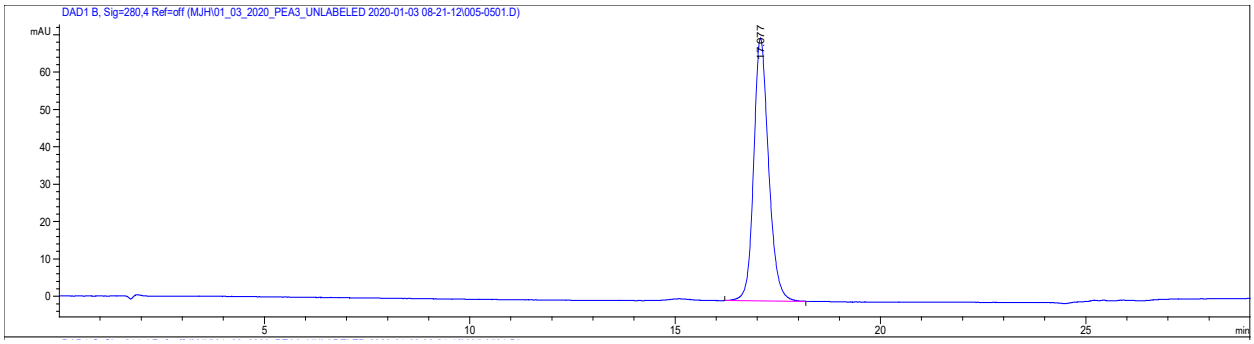

Analytical HPLC trace of **ETV4(45-76)^{H59Q}**, monitored at 280 nm. Analytical sample was run in a water (with 100 mM ammonium acetate)/ acetonitrile system. The sample was injected with an isocratic flow of 70% water (with 100 mM ammonium acetate) and 30% acetonitrile. After 2 min, the solvent gradient was increased from 10-35% acetonitrile over 20 min.

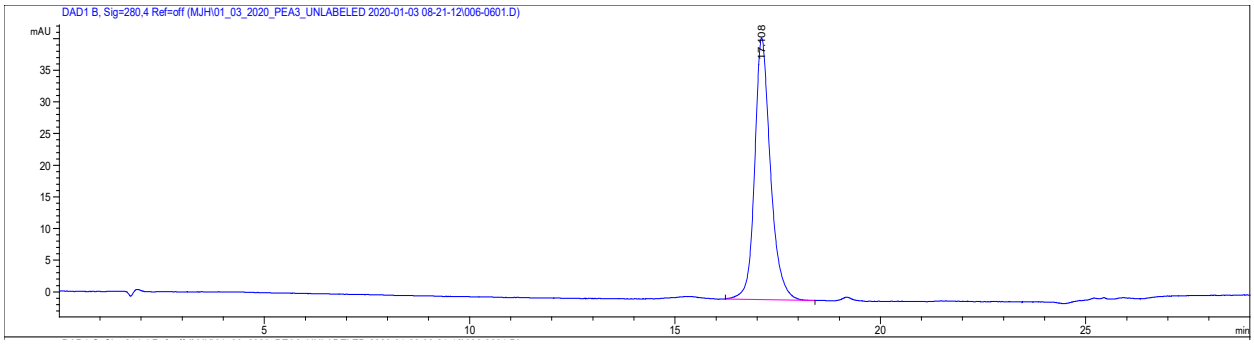

Analytical HPLC trace of **ETV4(45-76)^{L48V}**, monitored at 280 nm. Analytical sample was run in a water (with 100 mM ammonium acetate)/ acetonitrile system. The sample was injected with an isocratic flow of 70% water (with 100 mM ammonium acetate) and 30% acetonitrile. After 2 min, the solvent gradient was increased from 10-35% acetonitrile over 20 min.

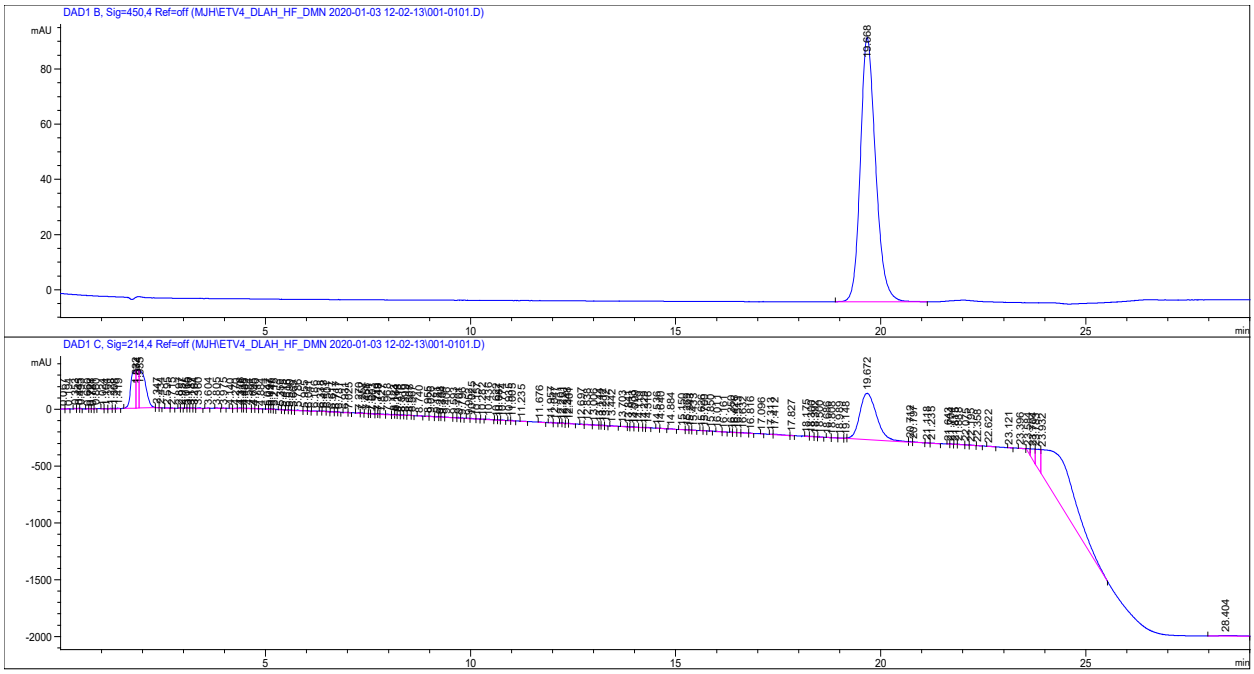

Analytical HPLC trace of **4-DMN-ETV1(38-69)**, monitored at 450 nm (above) and 214 nm (below). Analytical sample was run in a water (with 100 mM ammonium acetate)/ acetonitrile system. The sample was injected with an isocratic flow of 70% water (with 100 mM ammonium acetate) and 30% acetonitrile. After 2 min, the solvent gradient was increased from 10-35% acetonitrile over 20 min.

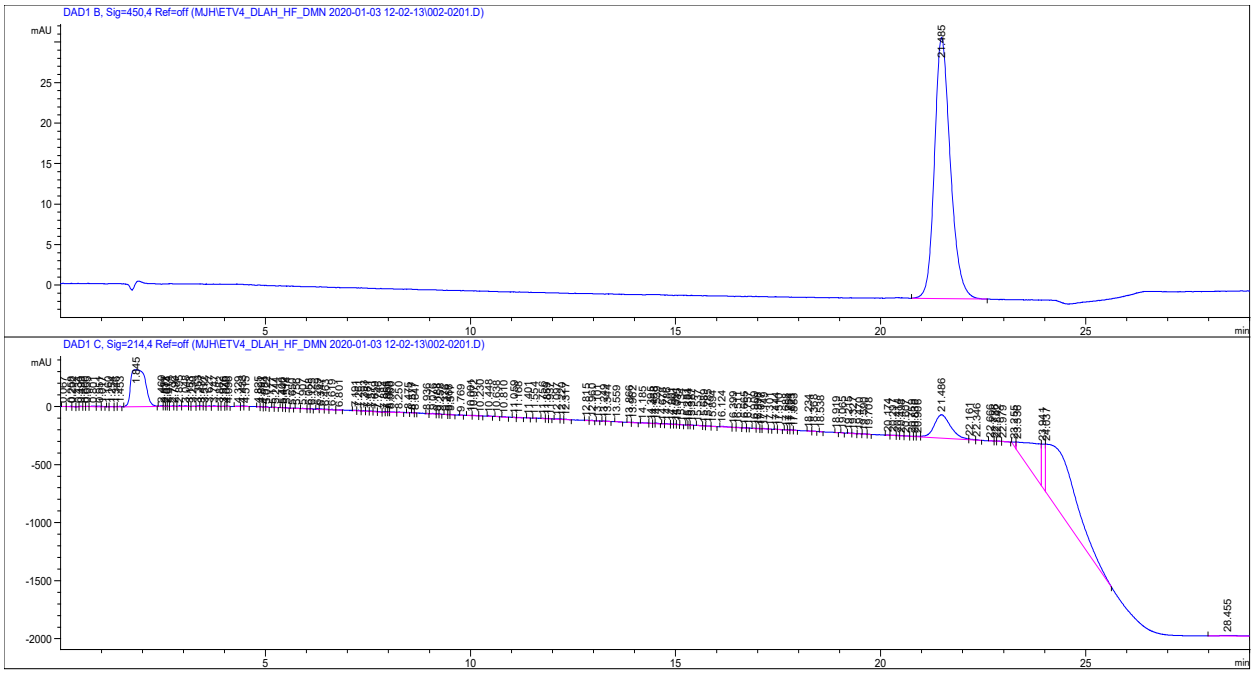

Analytical HPLC trace of **4-DMN-ETV4(45-76)**, monitored at 450 nm (above) and 214 nm (below). Analytical sample was run in a water (with 100 mM ammonium acetate)/ acetonitrile system. The sample was injected with an isocratic flow of 70% water (with 100 mM ammonium acetate) and 30% acetonitrile. After 2 min, the solvent gradient was increased from 10-35% acetonitrile over 20 min.

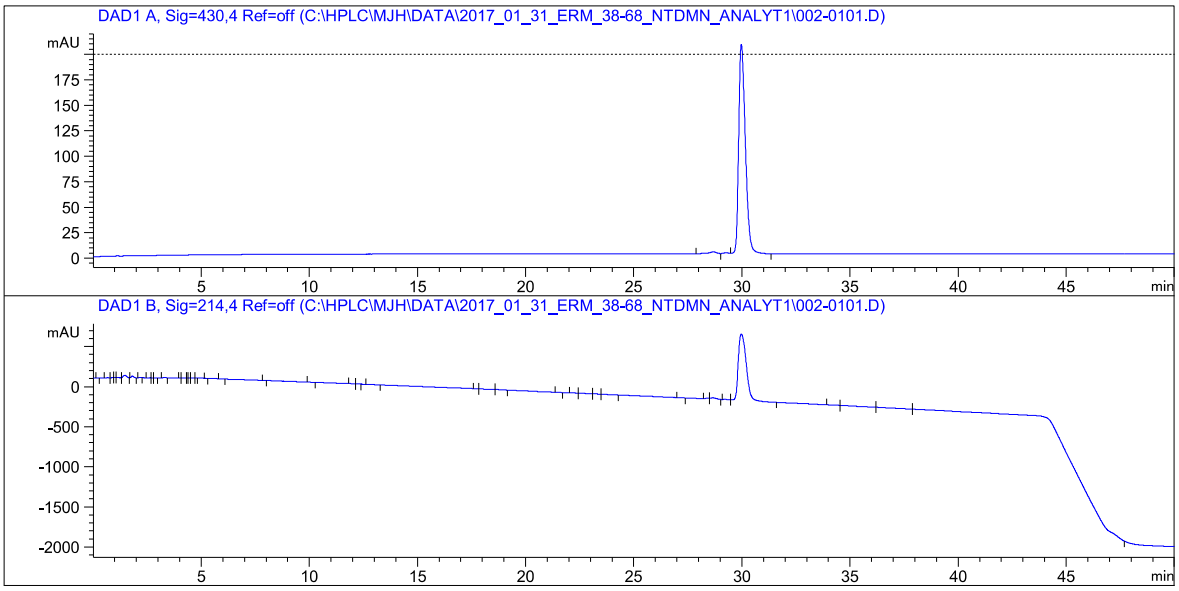

Analytical HPLC trace of **4-DMN-ETV5(38-68)**, monitored at 430 nm (above) and 214 nm (below). Analytical sample was run in a water (with 100 mM ammonium acetate)/ acetonitrile system. The sample was injected with an isocratic flow of 90% water (with 100 mM ammonium acetate) and 10% acetonitrile. After 2 min, the solvent gradient was increased from 10-40% acetonitrile over 40 min.

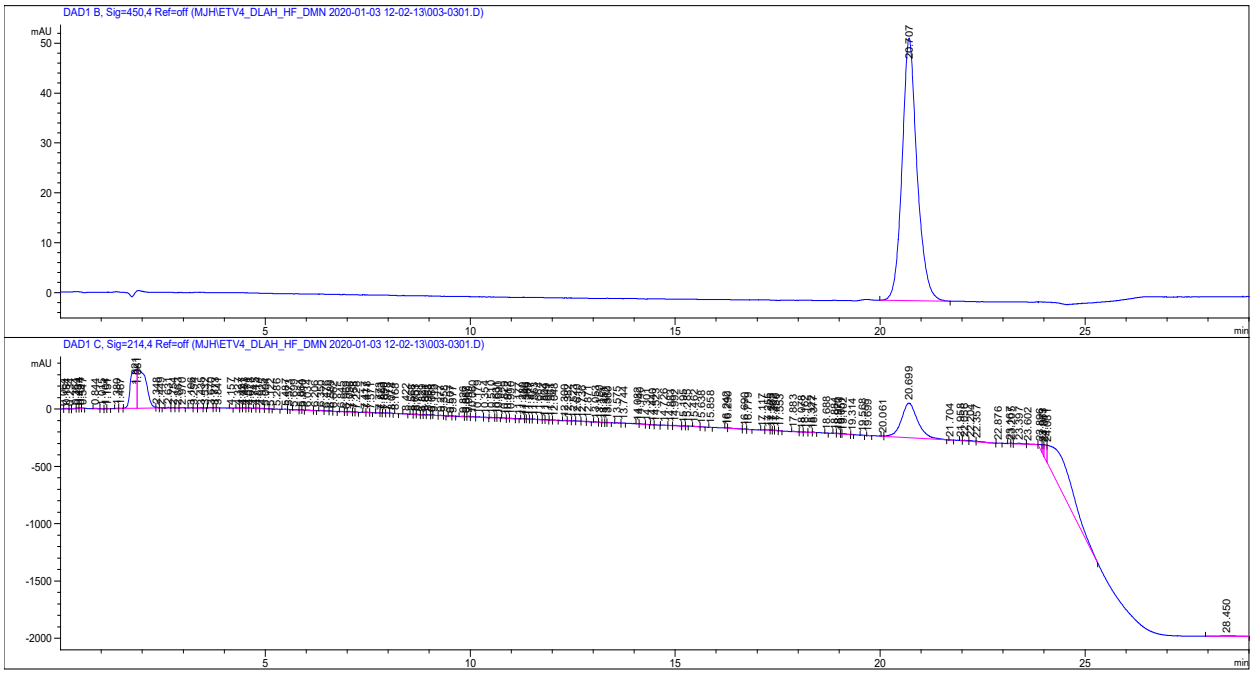

Analytical HPLC trace of **4-DMN-ETV4(45-76)$^{LPPL/QF}$**, monitored at 450 nm (above) and 214 nm (below). Analytical sample was run in a water (with 100 mM ammonium acetate)/ acetonitrile system. The sample was injected with an isocratic flow of 70% water (with 100 mM ammonium acetate) and 30% acetonitrile. After 2 min, the solvent gradient was increased from 10-35% acetonitrile over 20 min.

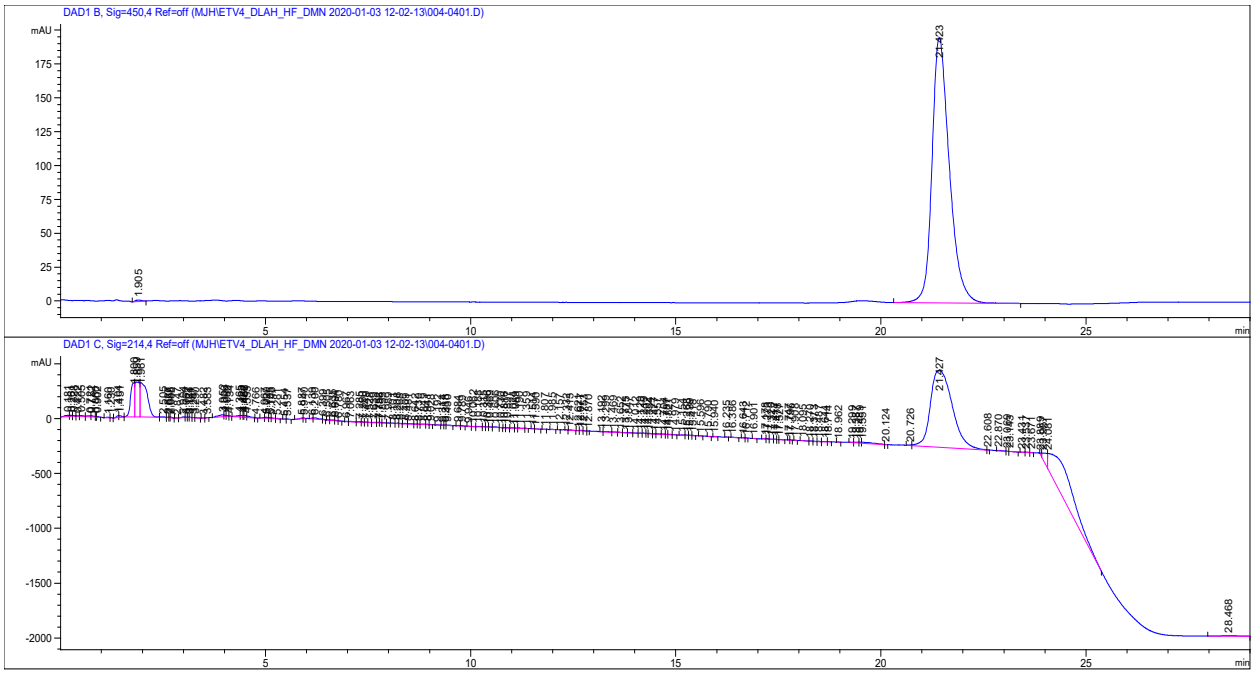

Analytical HPLC trace of **4-DMN-ETV4(45-76)$^{LPPL/HL}$**, monitored at 450 nm (above) and 214 nm (below). Analytical sample was run in a water (with 100 mM ammonium acetate)/ acetonitrile system. The sample was injected with an isocratic flow of 70% water (with 100 mM ammonium acetate) and 30% acetonitrile. After 2 min, the solvent gradient was increased from 10-35% acetonitrile over 20 min.

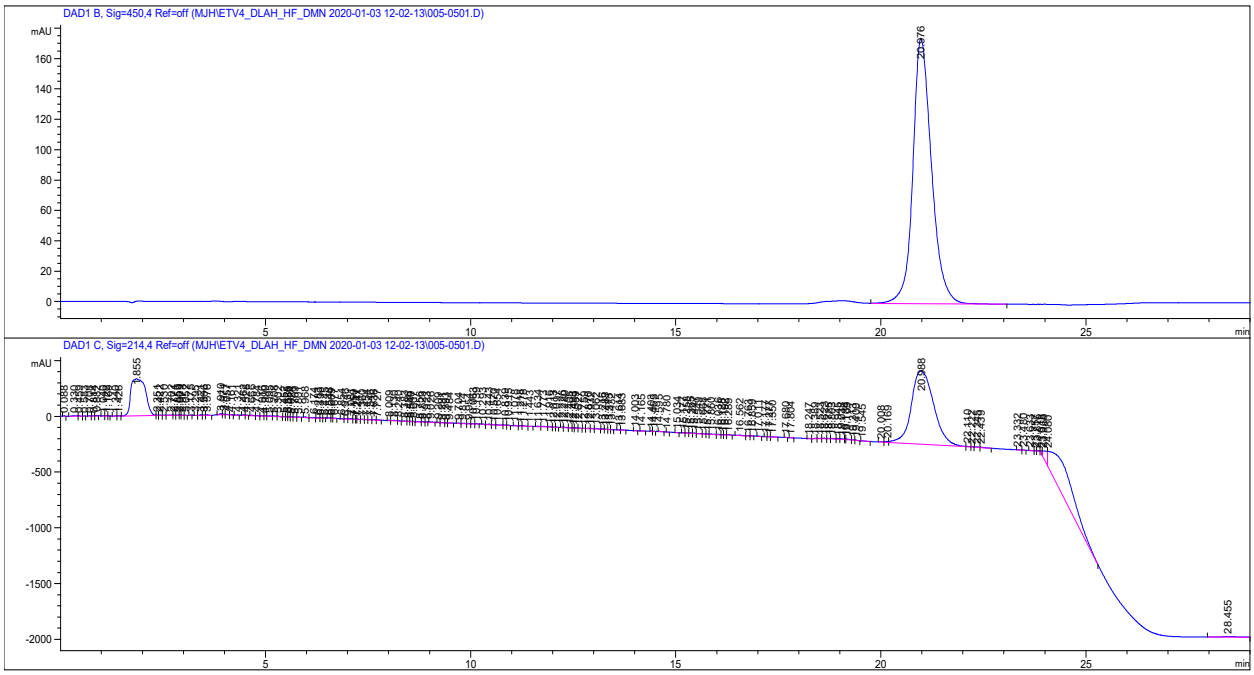

Analytical HPLC trace of **4-DMN-ETV4(45-76)$^{LPPL/QL}$**, monitored at 450 nm (above) and 214 nm (below). Analytical sample was run in a water (with 100 mM ammonium acetate)/ acetonitrile system. The sample was injected with an isocratic flow of 70% water (with 100 mM ammonium acetate) and 30% acetonitrile. After 2 min, the solvent gradient was increased from 10-35% acetonitrile over 20 min.

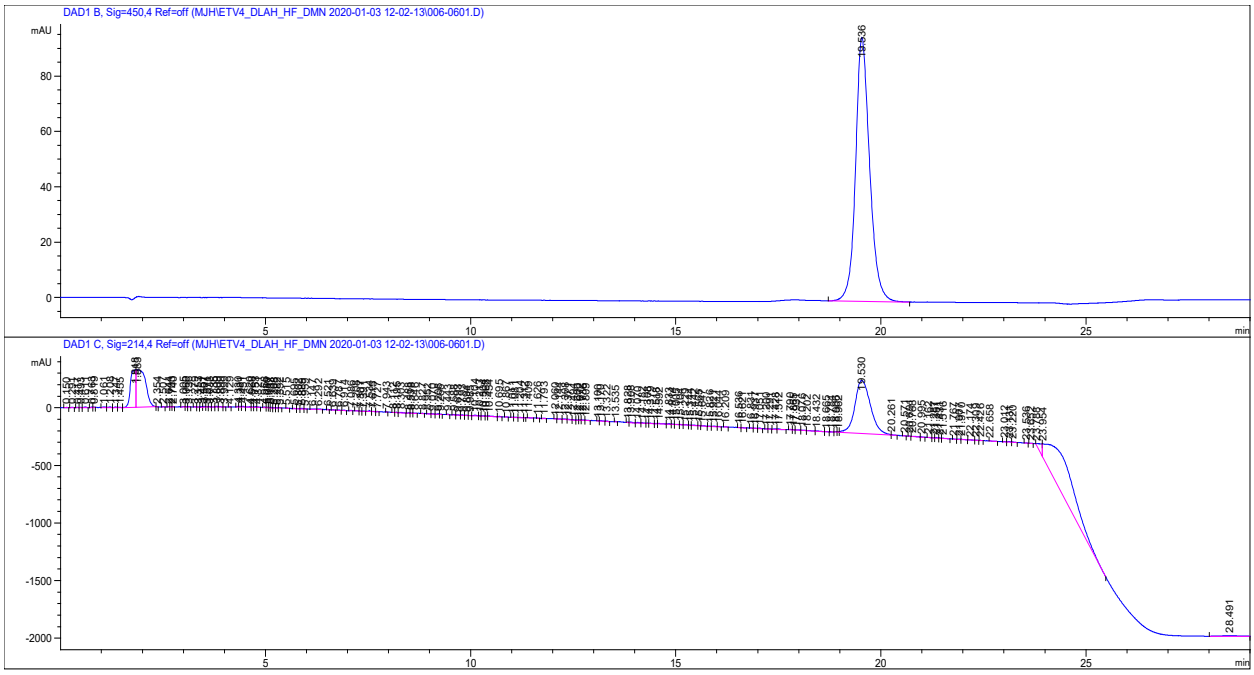

Analytical HPLC trace of **4-DMN-ETV4(45-76)$^{DLAH/HF}$**, monitored at 450 nm (above) and 214 nm (below). Analytical sample was run in a water (with 100 mM ammonium acetate)/ acetonitrile system. The sample was injected with an isocratic flow of 70% water (with 100 mM ammonium acetate) and 30% acetonitrile. After 2 min, the solvent gradient was increased from 10-35% acetonitrile over 20 min.

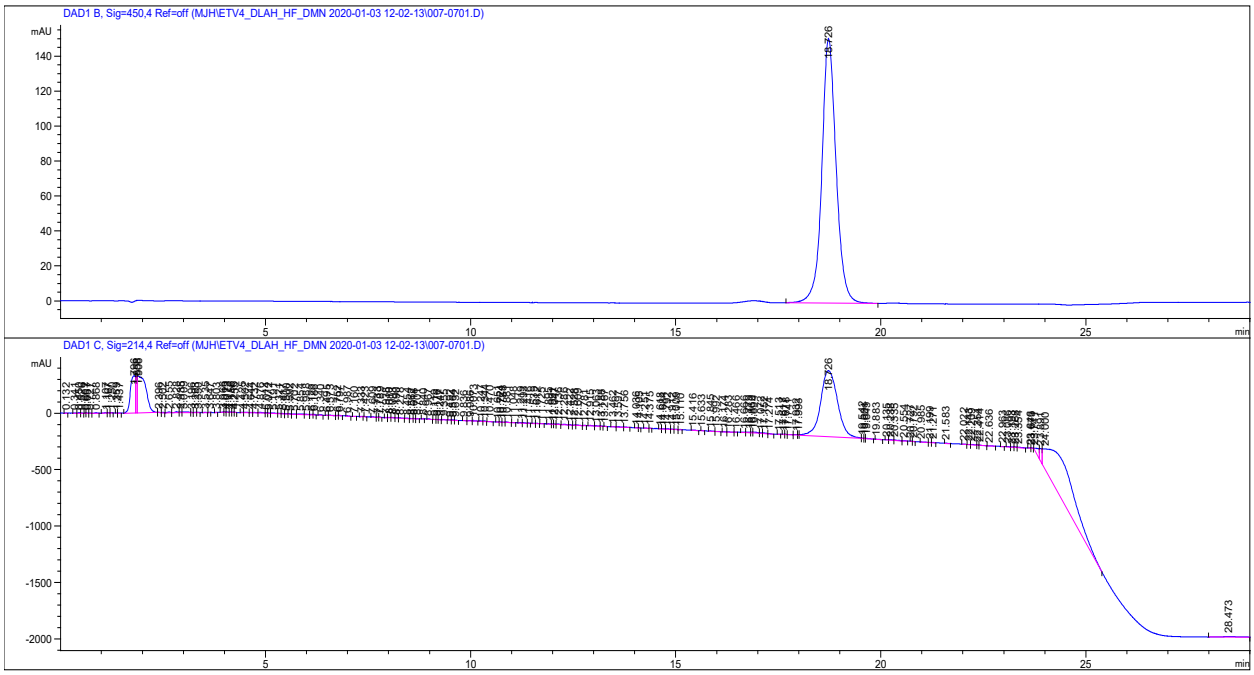

Analytical HPLC trace of **4-DMN-ETV4(45-76)$^{DLAH/QF}$**, monitored at 450 nm. Analytical sample was run in a water (with 100 mM ammonium acetate)/ acetonitrile system. The sample was injected with an isocratic flow of 70% water (with 100 mM ammonium acetate) and 30% acetonitrile. After 2 min, the solvent gradient was increased from 10-35% acetonitrile over 20 min.

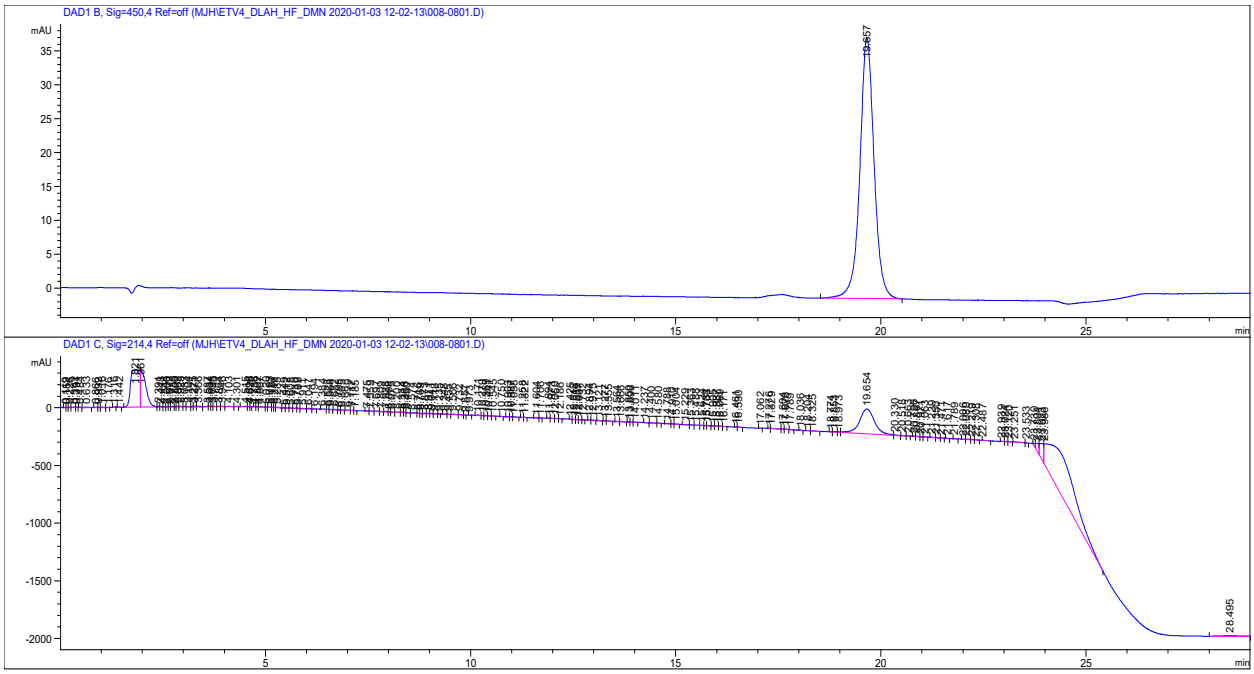

Analytical HPLC trace of **4-DMN-ETV4(45-76)$^{DLAH/HL}$**, monitored at 450 nm (above) and 214 nm (below). Analytical sample was run in a water (with 100 mM ammonium acetate)/ acetonitrile system. The sample was injected with an isocratic flow of 70% water (with 100 mM ammonium acetate) and 30% acetonitrile. After 2 min, the solvent gradient was increased from 10-35% acetonitrile over 20 min.

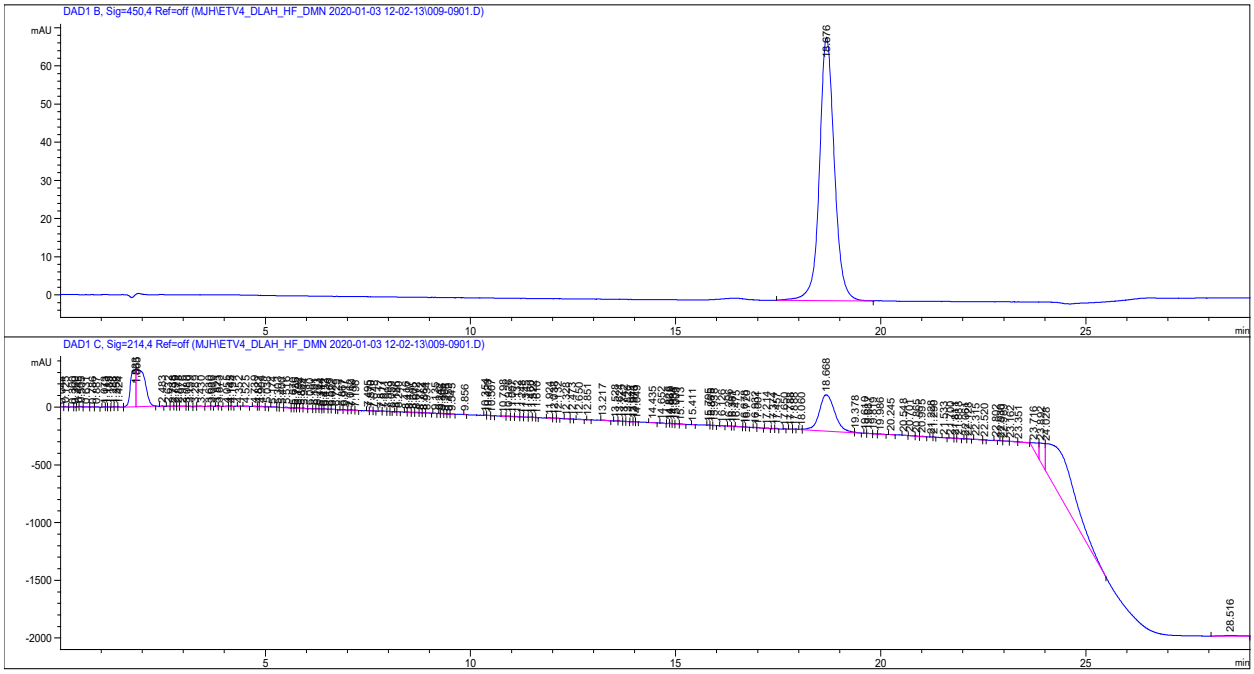

Analytical HPLC trace of **4-DMN-ETV1(42-69)**, monitored at 450 nm (above) and 214 nm (below). Analytical sample was run in a water (with 100 mM ammonium acetate)/ acetonitrile system. The sample was injected with an isocratic flow of 70% water (with 100 mM ammonium acetate) and 30% acetonitrile. After 2 min, the solvent gradient was increased from 10-35% acetonitrile over 20 min.

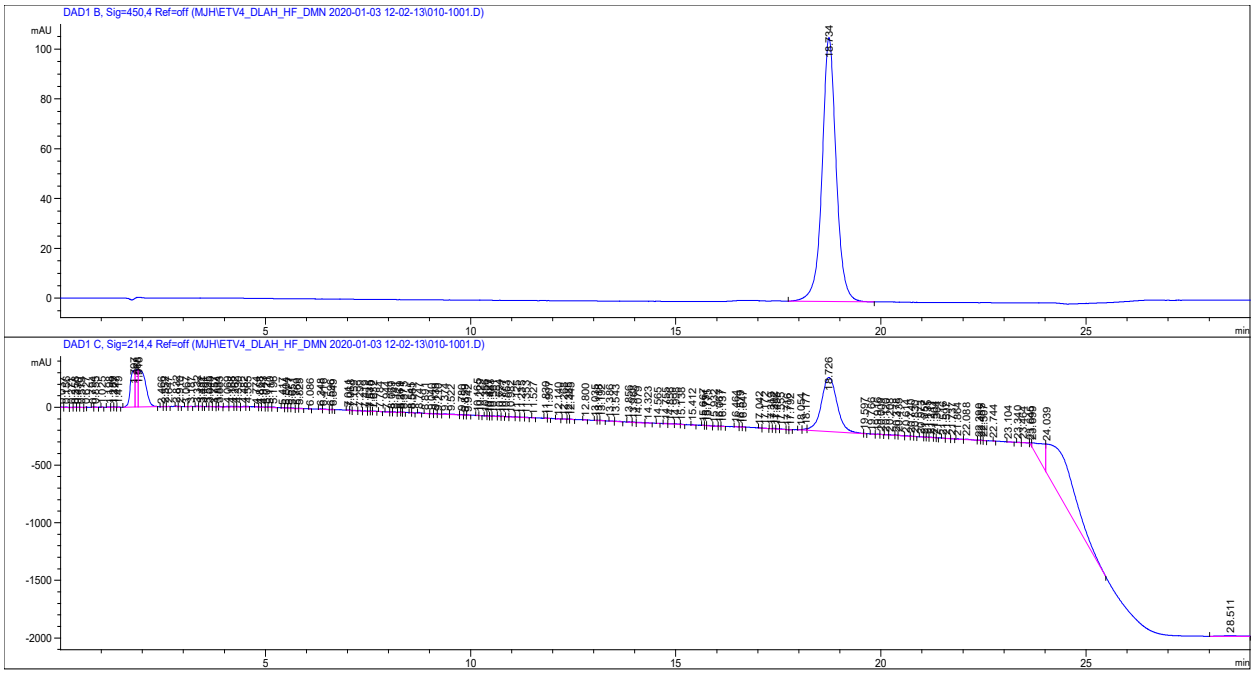

Analytical HPLC trace of **4-DMN-ETV4(49-76)**, monitored at 450 nm (above) and 214 nm (below). Analytical sample was run in a water (with 100 mM ammonium acetate)/ acetonitrile system. The sample was injected with an isocratic flow of 70% water (with 100 mM ammonium acetate) and 30% acetonitrile. After 2 min, the solvent gradient was increased from 10-35% acetonitrile over 20 min.

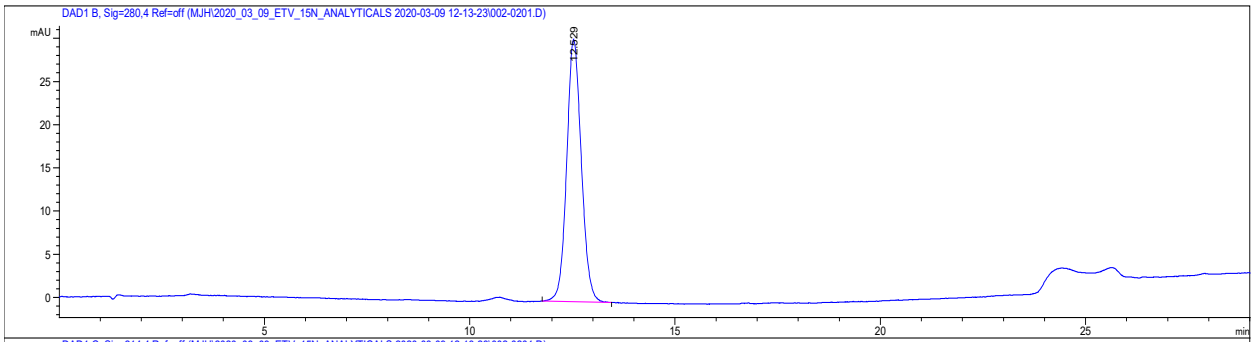

Analytical HPLC trace of **ETV1(38-69) ^{15}N-Leu39**, monitored at 280 nm. Analytical sample was run in a water (with 100 mM ammonium acetate)/ acetonitrile system. The sample was injected with an isocratic flow of 70% water (with 100 mM ammonium acetate) and 30% acetonitrile. After 2 min, the solvent gradient was increased from 10-35% acetonitrile over 20 min.

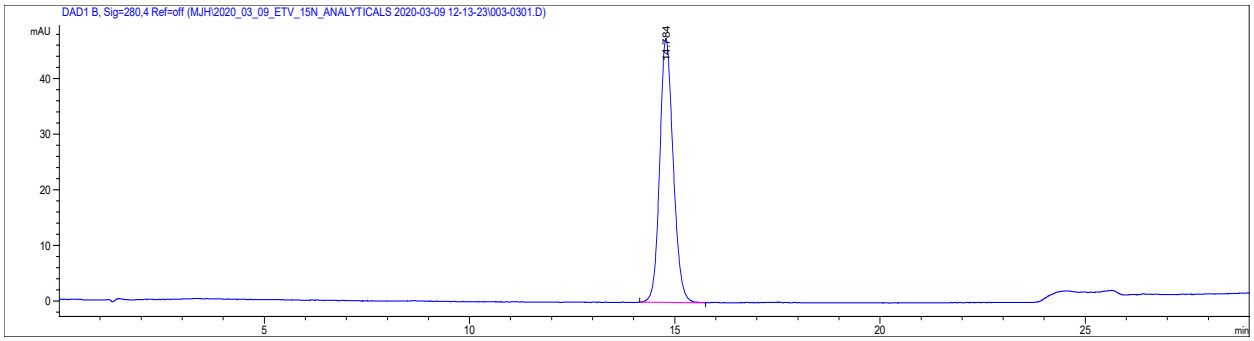

Analytical HPLC trace of **ETV4(45-76) ^{15}N-Leu48**, monitored at 280 nm. Analytical sample was run in a water (with 100 mM ammonium acetate)/ acetonitrile system. The sample was injected with an isocratic flow of 70% water (with 100 mM ammonium acetate) and 30% acetonitrile. After 2 mins, the solvent gradient was increased from 10-35% acetonitrile over 20 mins.

References

1. A. R. Henderson, *et al.*, Conservation of coactivator engagement mechanism enables small-molecule allosteric modulators. *Proc Natl Acad Sci USA* **115**, 8960–8965 (2018).

2. V. Muñoz, L. Serrano, Elucidating the folding problem of helical peptides using empirical parameters. *Nat Struct Mol Biol* **1**, 399–409 (1994).

3. F. Delaglio, *et al.*, NMRPipe: A multidimensional spectral processing system based on UNIX pipes. *J Biomol NMR* **6** (1995).

4. W. Lee, M. Tonelli, J. L. Markley, NMRFAM-SPARKY: enhanced software for biomolecular NMR spectroscopy. *Bioinformatics* **31**, 1325–1327 (2015).

5. M. Mobli, A. S. Stern, W. Bermel, G. F. King, J. C. Hoch, A non-uniformly sampled 4D HCC(CO)NH-TOCSY experiment processed using maximum entropy for rapid protein sidechain assignment. *Journal of Magnetic Resonance* **204**, 160–164 (2010).

6. A. G. Milbradt, *et al.*, Structure of the VP16 transactivator target in the Mediator. *Nat Struct Mol Biol* **18**, 410–415 (2011).

7. E. Vojnic, *et al.*, Structure and VP16 binding of the Mediator Med25 activator interaction domain. *Nat Struct Mol Biol* **18**, 404–409 (2011).